



# Spacecraft Drift Counteraction Optimal Control: Open-Loop and Receding Horizon Solutions

Robert A. E. Zidek\* and Ilya V. Kolmanovskiy†  
 University of Michigan, Ann Arbor, Michigan 48109

and

Alberto Bemporad‡  
 IMT School for Advanced Studies, 55100 Lucca, Italy

DOI: 10.2514/1.G002978

The objective of drift counteraction optimal control is to maximize the time that a given system satisfies prescribed constraints. This paper describes novel open-loop and receding horizon/model predictive control-based approaches to solve this problem. To illustrate the potential for drift counteraction optimal control applications to spacecraft operational life extension, two examples of geostationary satellite station keeping near the end of satellite operational life and spacecraft attitude control considering the effects of reaction wheel failures and reaction wheel speed saturation are presented. For the satellite station-keeping problem, the objective is to counteract drift imposed by orbital perturbations and maximize the time before prescribed position constraints are violated, given fuel limitations. For the attitude control problem, the spacecraft is subject to disturbances from solar radiation pressure; and tight pointing constraints need to be satisfied for as long as possible using reaction wheels. The cases of underactuated spacecraft (one or two reaction wheels) and fully actuated spacecraft are treated.

## Nomenclature

$A$	=	state matrix
$a$	=	acceleration, m/s <sup>2</sup>
$B$	=	control input matrix
$\mathcal{B}$	=	body-fixed frame
$b$	=	vector defining constraints; see Eq. (3)
$C$	=	matrix defining constraints; see Eq. (3)
$d$	=	disturbance
$F$	=	thrust force, N
$f$	=	nonlinear function
$\bar{G}$	=	set defining state constraints; see Eq. (3)
$\tilde{G}$	=	tightened state constraints; $\tilde{G} \subset \bar{G}$
$\tilde{g}$	=	reaction wheel spin axis resolved in $\mathcal{B}$ frame
$\mathcal{H}$	=	Hill's frame
$\mathcal{I}$	=	Earth-centered inertial frame
$J$	=	moment of inertia, kg/m <sup>2</sup>
$L_i$	=	length of cuboid spacecraft; $i \in \{x, y, z\}$ , m
$l_i$	=	distance between center of mass and geometric center; $i \in \{x, y, z\}$ , m
$M$	=	some large number
$m$	=	mass, kg
$N$	=	time horizon of mathematical program
$N_{\text{add}}$	=	parameter in Algorithms 1 and 2 to update $N$
$N_{\text{ub}}$	=	upper bound on $N$
$n_0$	=	geostationary equatorial orbit angular rate, rad/s
$p$	=	number of control inputs
$r$	=	position, m
$S$	=	skew-symmetric matrix; see Eq. (B1)
$U$	=	set defining control constraints
$U_{\text{seq}}$	=	set of admissible control sequences; see Eq. (2)
$u$	=	control input vector
$v$	=	velocity, m/s
$W$	=	matrix containing reaction wheel spin axes; see Eq. (B3)

$w$	=	weight in modified linear programming objective function; see Eqs. (27) and (40)
$x$	=	state vector
$\alpha$	=	angular acceleration, rad/s <sup>2</sup>
$\gamma$	=	additional linear programming variable
$\Delta t$	=	sampling time, s
$\Delta v_{\text{acc}}$	=	accumulated $\Delta v$ , m/s
$\delta$	=	integer-valued indicator variable for $x_t \notin G_t$
$\epsilon$	=	real-valued indicator variable for $x_t \notin G_t$
$\zeta$	=	additional linear programming variable
$\theta$	=	Euler angle (pitch), rad
$\mu$	=	gravitational parameter, m <sup>3</sup> /s <sup>2</sup>
$\nu$	=	reaction wheel spin rate, rad/s
$\tau$	=	first exit time; see Eq. (4)
$\tau_{\text{lb}}$	=	lower bound on optimal first exit time
$\tau_{\text{srp}}$	=	solar radiation pressure disturbance torque, N/m
$\tilde{\tau}$	=	first exit time with respect to tightened state constraints
$\Phi_S$	=	solar flux, W/m <sup>2</sup>
$\phi$	=	Euler angle (roll), rad
$\psi$	=	Euler angle (yaw), rad
$\omega$	=	angular velocity, rad/s

## Subscripts

$c$	=	control
$E$	=	Earth
GEO, 0	=	geostationary equatorial orbit reference orbit
$J_2$	=	$J_2$ perturbation
$M$	=	moon
$p$	=	orbital perturbations
recover	=	recovery controller defined by linear programming [Eq. (18)]
$S$	=	sun
SC	=	spacecraft
$s$	=	state
srp	=	solar radiation pressure
th	=	thrust

Received 16 April 2017; revision received 25 March 2018; accepted for publication 6 May 2018; published online 6 August 2018. Copyright © 2018 by the American Institute of Aeronautics and Astronautics, Inc. All rights reserved. All requests for copying and permission to reprint should be submitted to CCC at [www.copyright.com](http://www.copyright.com); employ the ISSN 0731-5090 (print) or 1533-3884 (online) to initiate your request. See also AIAA Rights and Permissions [www.aiaa.org/randp](http://www.aiaa.org/randp).

\*Ph.D. Candidate, Department of Aerospace Engineering.

†Professor, Department of Aerospace Engineering. Member AIAA.

‡Professor.

## I. Introduction

THE problem addressed in this paper can be stated as follows: given a deterministic system and a set of prescribed constraints on the system's process and control variables, find a control law that

maximizes the time before at least one of the constraints is violated. Such problems are referred to as drift counteraction optimal control (DCOC) problems because the solution may be viewed as counteracting drift imposed by disturbances or system dynamics in order to delay constraint violation. DCOC problems arise in many engineering systems [in particular, those with large persistent disturbances (e.g., wind gusts or drag), limited control authority (e.g., underactuated systems), or finite resources (fuel, energy, component life, etc.)], causing the process variables of the system to drift.

In this context, we consider systems represented by nonlinear discrete-time models of the form

$$x_{t+1} = f_t(x_t, u_t) \quad (1)$$

where  $x_t \in \mathbb{R}^n$  and  $u_t \in \mathbb{R}^p$  denote the state and control input vectors, respectively, at a time instant  $t \in \mathbb{Z}_{\geq 0}$ ; and  $f_t$  is a time-dependent nonlinear function. To avoid unnecessary technicalities, we assume  $f_t$  is defined over  $\mathbb{R}^n \times \mathbb{R}^p$  for all  $t \in \mathbb{Z}_{\geq 0}$ ; however, this assumption can be relaxed. The control is constrained as  $u_t \in U_t$ , where  $U_t = \{u \in \mathbb{R}^p: C_{c,t}u \leq b_{c,t}\}$  is a family of polyhedral sets. A control sequence is denoted by  $\{u_t\} = \{u_0, u_1, \dots\}$ , and

$$U_{\text{seq}} = \{\{u_t\}: u_t \in U_t \text{ for all } t \in \mathbb{Z}_{\geq 0}\} \quad (2)$$

is the set of admissible control sequences. Furthermore, suppose that a family of polyhedral sets

$$G_t = \{x \in \mathbb{R}^n: C_{s,t}x \leq b_{s,t}\} \quad (3)$$

is defined that one wants  $x_t$  to be inside, e.g.,  $x_t \in G_t$  corresponds to safe and efficient system operation. Then, given an initial  $x_0 \in G_0$  and the control sequence  $\{u_t\} \in U_{\text{seq}}$ , the corresponding first exit time is defined as

$$\tau(x_0, \{u_t\}) = \inf\{t \in \mathbb{Z}_{\geq 0}: x_t \notin G_t\} \quad (4)$$

where  $x_t$  is the response of Eq. (1) to the initial condition  $x_0$  and input sequence  $\{u_t\}$ . The DCOC problem is given by

$$\begin{aligned} & \max_{\{u_t\} \in U_{\text{seq}}} \tau(x_0, \{u_t\}) \\ & \text{subject to } x_{t+1} = f_t(x_t, u_t) \end{aligned} \quad (5)$$

Related problems were studied in continuous time in [1–9]. In contrast to problem (5), however, most of the previous research considered discounted cost/yield functions instead of explicitly maximizing the first exit time. Moreover, the continuous-time formulation requires solving the Hamilton–Jacobi–Bellman equation, which is a partial differential equation (PDE) for which explicit solutions can only be obtained in some special cases. The discrete-time version in Eq. (5), on the other hand, is computationally more tractable as compared to numerically solving a PDE.

In [10], problem (5) was solved using dynamic programming techniques. Due to the curse of dimensionality, this approach is limited to lower-dimensional problems. To solve higher-dimensional problems, a new approach using linear programming (LP) was developed in [11] for DCOC based on linear models of the form  $x_{t+1} = A_t x_t + B_t u_t + d_t$ . It was shown in [11] that the solution to the linear DCOC problem reduced to the solution of a mixed-integer linear program (MILP). Moreover, good-quality suboptimal solutions can be obtained by solving a similar program without integer variables using standard LP. The LP formulation for the linear DCOC problem was used to implement a model predictive control (MPC) strategy in [12] to approximate the solution to a nonlinear spacecraft attitude DCOC problem.

The main contribution of this paper is a mixed-integer nonlinear program (MINLP) formulation that solves problem (5) as well as a

similar nonlinear program (NLP) formulation without integer variables that yields good-quality suboptimal solutions. Moreover, we improve the LP-based MPC method from previous conference papers [11,12] to generate effective state feedback solutions for nonlinear systems and demonstrate the potential for the use of DCOC for spacecraft operational life extension. Along these lines, we treat two different DCOC applications to geostationary satellite station keeping and to spacecraft attitude control. In both problems, we compare the NLP solution with the LP-based MPC solution simulated on the nonlinear model.

The station-keeping problem assumes a satellite is in geostationary equatorial orbit (GEO) subject to several orbital perturbations. The satellite is equipped with thrusters that consume a specified amount of fuel. Given an initial amount of fuel, the objective is to find a thrust strategy for which prescribed constraints on the satellite position are satisfied for as long as possible (i.e., before running out of fuel). Previous station-keeping approaches addressed this objective by scheduling thrust maneuvers either periodically to compensate the perturbing forces or whenever the satellite was about to exit its prescribed position window [13–18]. Other approaches were based on tracking the center of the prescribed position window using feedback control techniques [19,20]. In contrast, our approach directly addresses the station-keeping objective by explicitly maximizing the time until constraint violation (i.e., until exiting the position window).

For the spacecraft attitude control problem, reaction wheels (RWs) are used to counteract drift caused by solar radiation pressure (SRP) disturbance torques [12]. We consider the cases of an underactuated spacecraft (one or two operable RWs) as well as of a fully actuated spacecraft (three operable RWs) with one RW being nearly saturated. In both cases, the control authority is limited. Thus, depending on the initial condition, prescribed orientation constraints will eventually be violated, and the control objective is to delay this event. This case study is motivated by frequent situations, such as for the Kepler spacecraft [21,22], in which tight pointing constraints must be satisfied to be able to image when RWs have failed. Similar to the GEO station-keeping problem, the advantage of our approach over previous approaches [23–27] is that it explicitly maximizes the time until prescribed orientation constraints are violated.

The structure of the paper is as follows. In Sec. II, nonlinear programs are developed that yield open-loop solutions and good-quality approximate solutions to problem (5). Section III presents the MPC scheme for closed-loop control. Numerical case studies for the GEO station-keeping and spacecraft attitude DCOC problems are treated in Sec. IV. A conclusion is given in Sec. V.

Throughout the paper, we assume that the initial state vector satisfies the constraints, i.e.,  $x_0 \in G_0$ . Moreover, we make the following assumption:

*Assumption 1:* There exists  $\bar{T} > 0$  such that  $\tau(x, \{u_t\}) \leq \bar{T}$  for all  $x \in G_0$  and  $\{u_t\} \in U_{\text{seq}}$ .

Assumption 1 is reasonable in many applications in which finite resources, such as fuel, are of concern (e.g., GEO station keeping; Sec. IV.A) or the control authority of the system is limited (e.g., underactuated spacecraft attitude control; Sec. IV.B). A solution to problem (5), which may not be unique (see, e.g., [11]), exists under Assumption 1, as stated in the following theorem.

*Theorem 1:* Suppose Assumption 1 holds. Then, a solution to problem (5) exists for all  $x \in G_0$ .

*Proof:* Let  $x = x_0 \in G_0$  be a given initial condition. Moreover, note that the objective function in Eq. (5) is integer valued and bounded (by Assumption 1). Because any bounded collection of integers has a maximum, the solution existence to problem (5) follows.  $\square$

## II. Open-Loop Solutions

A solution to problem (5) may be obtained by solving the following MINLP:

$$\begin{aligned}
& \min_{\{u_t\}, \{\delta_{\tau_{lb}}, \dots, \delta_N\}} \sum_{t=\tau_{lb}}^N \delta_t \\
& \text{subject to } x_{t+1} = f_t(x_t, u_t) \\
& \delta_{t-1} \leq \delta_t \\
& \delta_t \in \{0, 1\} \subset \mathbb{Z}, t \in \{\tau_{lb}, \dots, N\} \\
& C_{s,t}x_t \leq b_{s,t}, t \in \{1, \dots, \tau_{lb} - 1\} \\
& C_{s,t}x_t \leq b_{s,t} + \mathbf{1}M\delta_t, t \in \{\tau_{lb}, \dots, N\} \\
& u_t \in U_t
\end{aligned} \tag{6}$$

where the binary variables  $\delta_t$  indicate when  $x_t \notin G_t$  and  $\tau_{lb}$  is a lower bound on the optimal first exit time, i.e.,

$$1 \leq \tau_{lb} \leq \tau(x_0, \{u_t^*\}) \tag{7}$$

where  $\{u_t^*\}$  is a solution to Eq. (5). Note that  $\tau_{lb}$  can be chosen as the first exit time of any trajectory generated by an admissible control law. Moreover, the symbol  $\mathbf{1}$  in Eq. (6) denotes the  $n$ -dimensional vector of ones,  $M$  is a constant scalar, and the time horizon of the MINLP is given by  $N$ .

Theorem 2 provides conditions under which the solutions of problem (5) and MINLP (6) are equivalent. In the following, a state trajectory [corresponding to a control sequence  $\{u_t\}$  and the dynamics  $x_{t+1} = f_t(x_t, u_t)$ ] is denoted by  $\{x_t\}$ , where  $x_0 \in G_0$ . Moreover, we make the following assumption about  $M$  and the time horizon  $N$ .

*Assumption 2:* The time horizon of MINLP (6) is sufficiently large that  $N \geq \tau(x_0, \{u_t\})$  for all  $\{u_t\} \in U_{\text{seq}}$ . Moreover,  $M$  in Eq. (6) is sufficiently large that, for any  $\{u_t\} \in U_{\text{seq}}$  with corresponding  $\{x_t\}$ ,  $C_{s,t}x_t \leq b_{s,t} + \mathbf{1}M$  for all  $t \in \{\tau_{lb}, \dots, N\}$ .

*Theorem 2:* Suppose Assumptions 1–2 hold. Then, the solutions to problem (5) and MINLP (6) are equivalent.

*Proof:* For the first part of the proof, we need to show that a solution to Eq. (6) is also a solution to Eq. (5). Let  $x_0 \in G_0$  be a given initial condition. Due to Assumption 1 and Eq. (7), there exists at least one control sequence  $\{u_t\} \in U_{\text{seq}}$  with corresponding  $\{x_t\}$  and a first exit time of  $\tau(x_0, \{u_t\}) \geq \tau_{lb}$ . Hence, because  $M$  is sufficiently large by Assumption 2,  $\delta_t \equiv 1$  is feasible together with  $\{u_t\}$  and  $\{x_t\}$ . Because the number of possible  $\delta_t$  sequences is finite and a feasible solution exists for at least one of them, a solution to Eq. (6) exists. Now, suppose that  $(\{u_t^{\text{NP}}\}, \{\delta_t^{\text{NP}}\})$  is a solution to MINLP (6), i.e.,

$$\sum_{t=\tau_{lb}}^N \delta_t^{\text{NP}} \leq \sum_{t=\tau_{lb}}^N \delta_t' \tag{8}$$

for all  $(\{u_t'\}, \{\delta_t'\})$  that satisfy the constraints in Eq. (6). Moreover, for any  $\{u_t'\} \in U_{\text{seq}}$ , let  $\{\bar{\delta}_t'\}$  be such that  $\bar{\delta}_t' = 0$  if  $t < \tau(x_0, \{u_t'\})$ , which is always feasible with respect to Eq. (6) due to  $M$  being sufficiently large (Assumption 2). Consequently, because  $N$  is sufficiently large according to Assumption 2,

$$\tau(x_0, \{u_t'\}) = \tau_{lb} + \sum_{t=\tau_{lb}}^N (1 - \bar{\delta}_t') = N + 1 - \sum_{t=\tau_{lb}}^N \bar{\delta}_t' \tag{9}$$

Hence, by Eqs. (8) and (9),

$$\begin{aligned}
\tau(x_0, \{u_t^{\text{NP}}\}) &= \min\{t: \delta_t^{\text{NP}} = 1\} \\
&= \tau_{lb} + \sum_{t=\tau_{lb}}^N (1 - \delta_t^{\text{NP}}) \\
&= N + 1 - \sum_{t=\tau_{lb}}^N \delta_t^{\text{NP}} \\
&\geq N + 1 - \sum_{t=\tau_{lb}}^N \bar{\delta}_t' = \tau(x_0, \{u_t'\}) \tag{10}
\end{aligned}$$

for all  $\{u_t'\} \in U_{\text{seq}}$ . It follows that  $\{u_t^{\text{NP}}\}$  is also a solution to problem (5).

For the second part of the proof, we need to show that a solution to problem (5), which exists due to Assumption 1 and Theorem 1, is also a solution to MINLP (6). Suppose  $\{u_t^*\}$  is a solution to Eq. (5). Thus,

$$\tau(x_0, \{u_t^*\}) \geq \tau(x_0, \{u_t'\}) \tag{11}$$

for all  $\{u_t'\} \in U_{\text{seq}}$ . Then, Eqs. (3) and (4), the constraints in Eq. (6), and  $N \geq \tau(x_0, \{u_t\})$  for all  $\{u_t\} \in U_{\text{seq}}$  (Assumption 2) imply that  $\delta_t^* = 1$  for  $t \in \{\tau(x_0, \{u_t^*\}), \dots, N\}$  and  $\delta_t' = 1$  for  $t \in \{\tau(x_0, \{u_t'\}), \dots, N\}$ , where  $\{\delta_t^*\}$  and  $\{\delta_t'\}$  are the solutions to MINLP (6) for  $\{u_t\} = \{u_t^*\}$  or  $\{u_t\} = \{u_t'\}$ , respectively, fixed. Assuming that the lower bound in Eq. (6) satisfies  $\tau_{lb} \leq \tau(x_0, \{u_t'\})$ , it follows that  $\delta_t^* = 0$  for  $\tau_{lb} \leq t < \tau(x_0, \{u_t^*\})$  and  $\delta_t' = 0$  for  $\tau_{lb} \leq t < \tau(x_0, \{u_t'\})$ . This and Eq. (11) imply that

$$\begin{aligned}
\sum_{t=\tau_{lb}}^N \delta_t^* &= \sum_{t=\tau_{lb}}^{\tau(x_0, \{u_t^*\})-1} \delta_t^* + \sum_{t=\tau(x_0, \{u_t^*\})}^N \delta_t^* \\
&= N + 1 - \tau(x_0, \{u_t^*\}) \\
&\leq N + 1 - \tau(x_0, \{u_t'\}) = \sum_{t=\tau_{lb}}^N \delta_t' \tag{12}
\end{aligned}$$

for all  $(\{u_t'\}, \{\delta_t'\})$  that satisfy the constraints of MINLP (6). Thus,  $(\{u_t^*\}, \{\delta_t^*\})$  is a solution to MINLP (6).  $\square$

The MINLP is in the class of NP-complete problems. Moreover, to the best of our knowledge, there exist no algorithms that can solve MINLPs with nonconvex constraints [such as  $x_{t+1} = f_t(x_t, u_t)$ ]. Therefore, the solution to MINLP (6) is approximated by a similar NLP without integer variables. The NLP is obtained by replacing the binary variables  $\delta_t$  in MINLP (6) with nonnegative real variables  $\varepsilon_t$ , yielding NLP (13).

$$\begin{aligned}
& \min_{\{u_t\}, \{\varepsilon_{\tau_{lb}}, \dots, \varepsilon_N\}} \sum_{t=\tau_{lb}}^N \varepsilon_t \\
& \text{subject to } x_{t+1} = f_t(x_t, u_t) \\
& 0 \leq \varepsilon_{t-1} \leq \varepsilon_t \\
& C_{s,t}x_t \leq b_{s,t}, t \in \{1, \dots, \tau_{lb} - 1\} \\
& C_{s,t}x_t \leq b_{s,t} + \mathbf{1}\varepsilon_t, t \in \{\tau_{lb}, \dots, N\} \\
& u_t \in U_t
\end{aligned} \tag{13}$$

*Remark 1:* In contrast to MINLP (6), in general, the solution to NLP (13) is suboptimal with respect to problem (5). However, if the time horizon satisfies  $N = \tau(x, \{u_t^*\}) - 1$ , where  $\tau(x, \{u_t^*\})$  is the optimal first exit time for problem (5), the solution to NLP (13) is optimal with respect to problem (5). Moreover, the solution to NLP (13) is close to a solution of problem (5) (in terms of first exit time performance) if  $N$  and  $\tau_{lb}$  are close to  $\tau(x, \{u_t^*\})$ . This is because the first exit time of  $\tau(x, \{u_t\})$ , corresponding to the NLP solution, satisfies either

$$\begin{aligned}
\tau(x, \{u_t\}) &\in \{\tau_{lb}, \dots, N, \dots, \tau(x, \{u_t^*\})\} \text{ if } N < \tau(x, \{u_t^*\}), \\
\tau(x, \{u_t\}) &= \tau(x, \{u_t^*\}) \text{ if } N = \tau(x, \{u_t^*\}), \text{ or} \\
\tau(x, \{u_t\}) &\in \{\tau_{lb}, \dots, \tau(x, \{u_t^*\})\} \text{ if } N < \tau(x, \{u_t^*\})
\end{aligned}$$

More information on this can be found in [28]. Detailed instructions on how to select  $N$  and  $\tau_{lb}$  for NLP (13) will be given in Sec. IV.

### III. MPC Strategy

After discussing open-loop solutions to problem (5) in the previous section, this section focuses on an MPC implementation. Due to the availability of efficient and robust solvers for linear programs, the

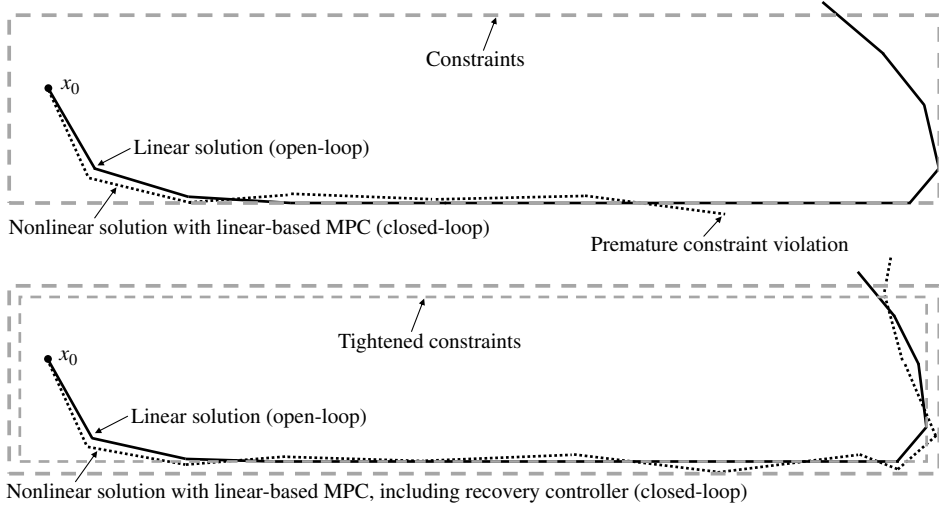


**Fig. 1** Illustration of effects of constraint tightening and recovery controller when linear-based control is applied to the nonlinear model. **Top:** state trajectories without constraint tightening. **Bottom:** state trajectories with constraint tightening [see (14)] and recovery controller [see LP (18)].

MPC scheme is based on a linear model approximation of the nonlinear system model, in which the linear model may be obtained by linearizing the nonlinear model in Eq. (5) about a proper reference trajectory and adding a time-varying disturbance term  $d_t$ . By recomputing the solution to the corresponding linear DCOC problem over a receding time horizon based on the current state vector, feedback is provided to compensate for unmodeled effects not present in the linear model.

However, as outlined in the top of Fig. 1, this linear-based MPC scheme may violate constraints ( $x_t \notin G_t$ ) prematurely when applied to the nonlinear system: in particular, when  $x_t$  is close to the boundary of  $G_t$ . This is due to potential unmodeled effects not present in the linear model and may be prevented by sufficiently tightening the state constraints for control computation, meaning the control input at each time instant is obtained by solving the linear DCOC problem with respect to tightened state constraints in order to create a margin of safety. In analogy to Eqs. (3) and (4), the tightened state constraints are defined by

$$\tilde{G}_t = \{x \in \mathbb{R}^n : \tilde{C}_{s,t}x \leq \tilde{b}_{s,t}\} \subset G_t \quad (14)$$

for all  $t \in \mathbb{Z}_{\geq 0}$ , and the corresponding first exit time is given by

$$\tilde{\tau}(x_0, \{u_t\}) = \inf\{t \in \mathbb{Z}_{\geq 0} : x_t \notin \tilde{G}_t\} \quad (15)$$

Note that the required margin for  $\tilde{G}_t$  depends on the accuracy of the linear model approximation (near the boundary of  $G_t$ ) and needs to be chosen based on the maximum difference between the linear model prediction of  $x_{t+1}$  and the actual response of the nonlinear system. Furthermore, the margin should not be greater than required because control performance may decrease otherwise due to unnecessary conservatism. Initial numerical tests may be required to choose a proper margin (as done for the numerical case studies in Sec. IV).

The linear DCOC problem (with respect to the tightened state constraints) is as follows:

$$\begin{aligned} & \max_{\{u_t\} \in U_{\text{seq}}} \tilde{\tau}(x_0, \{u_t\}) \\ & \text{subject to } x_{t+1} = A_t x_t + B_t u_t + d_t \end{aligned} \quad (16)$$

where  $x_0 \in \tilde{G}_0$ ,  $A_t \in \mathbb{R}^{n \times n}$ ,  $B_t \in \mathbb{R}^{n \times p}$ , and  $d_t \in \mathbb{R}^n$ . As shown in [11], a mixed-integer linear program provides a solution to the linear DCOC problem [Eq. (16)] under suitable assumptions. However, the MILP is in the class of NP-complete problems, and the worst-case computation time grows exponentially with the number of integer variables [11,29,30]. Consequently, efficient and robust computation

of a solution to Eq. (16) cannot be guaranteed with the MILP. Therefore, a solution to the linear DCOC problem [Eq. (16)] is approximated by solving a standard LP without integer variables. The LP is obtained by replacing the integer variables of the MILP in [11] with nonnegative real variables  $\varepsilon_t$ , which lead to the following LP for which efficient and robust solvers exist:

$$\begin{aligned} & \min_{\{u_t\}, \{\varepsilon_{\tau_{\text{lb}}}, \dots, \varepsilon_N\}} \sum_{t=\tau_{\text{lb}}}^N \varepsilon_t \\ & \text{subject to } x_{t+1} = A_t x_t + B_t u_t + d_t \\ & 0 \leq \varepsilon_{t-1} \leq \varepsilon_t \\ & \tilde{C}_{s,t} x_t \leq \tilde{b}_{s,t}, t \in \{1, \dots, \tau_{\text{lb}} - 1\} \\ & \tilde{C}_{s,t} x_t \leq \tilde{b}_{s,t} + \mathbf{1} \varepsilon_t, t \in \{\tau_{\text{lb}}, \dots, N\} \\ & u_t \in U_t \end{aligned} \quad (17)$$

where  $x_0 \in \tilde{G}_0$  and  $\varepsilon_t \in \mathbb{R}_{\geq 0}$ .

The solution of LP (17) is generally suboptimal with respect to the linear DCOC problem [Eq. (16)]. On the other hand, our previous numerical studies [11] showed that the LP solution was close or identical to the MILP/linear DCOC solution for proper choices of the time horizon  $N$  and upper bound  $\tau_{\text{lb}}$  on the optimal first exit time. As for NLP (13) and problem (5) [see Remark 1], the solution to LP (17) is close to a solution to the linear DCOC problem [Eq. (16)] if  $N$  and  $\tau_{\text{lb}}$  are close to  $\tilde{\tau}(x_0, \{u_t^*\})$ , where  $\{u_t^*\}$  is a solution to the linear DCOC problem [Eq. (16)].

Because the optimal first exit time  $\tilde{\tau}(x_0, \{u_t^*\})$  is a priori unknown, an iterative procedure was developed in [11] that effectively adjusted  $N$  while reducing the number of decision variables  $\varepsilon_t$  (by adjusting  $\tau_{\text{lb}}$ ) until a proper  $N$  was found. A similar procedure is outlined in Algorithm 1. In step 1 of Algorithm 1, the lower bound  $\tau_{\text{lb}}$  is initialized. The time horizon  $N$  is set in step 2 by adding a constant integer  $N_{\text{add}}$  to  $\tau_{\text{lb}}$ . Then, LP (17) is solved in step 3. Step 5 determines if constraint violation occurs (i.e., if there exists  $\varepsilon_t > 0$ ), which is equivalent to  $\varepsilon_N > 0$  due to the constraints  $\varepsilon_{t-1} \leq \varepsilon_t$  in Eq. (17). If no

**Algorithm 1** Iterative procedure to update  $N$  and  $\tau_{\text{lb}}$

- 
- 1:  $\tau_{\text{lb}} \leftarrow$  set initial lower bound
  - 2:  $N \leftarrow \tau_{\text{lb}} + N_{\text{add}}, N_{\text{add}} \in \mathbb{Z}_+$
  - 3:  $\{u_t\}, \{\varepsilon_{\tau_{\text{lb}}}, \dots, \varepsilon_N\} \leftarrow$  solution of LP (17)
  - 4:  $\tau \leftarrow \max\{t \leq N : \varepsilon_t = 0\} + 1$
  - 5: **if**  $\varepsilon_N = 0$ , **then**
  - 6:      $\tau_{\text{lb}} \leftarrow \tau$ ; go to step 2
  - 7: **end if**
-

constraint violation occurs ( $\varepsilon_t \equiv 0$ ), the lower bound is increased based on the current solution (steps 4 and 6). Going back to step 2, the procedure is repeated for an increased  $N$  until a constraint violation eventually occurs as a consequence of Assumption 1.

In addition to solving the linear DCOC problem with respect to the tightened state constraints, we augment the MPC strategy by a controller that tries to recover  $x_t \in \tilde{G}_t$  when the tightened state constraints are violated. This controller, which we refer to as the recovery controller, is described by the following LP:

$$\begin{aligned} \min_{\{u_t, \varepsilon_t\}} \quad & \sum_{t=1}^{N_{\text{recover}}} \varepsilon_t \\ \text{subject to} \quad & x_{t+1} = A_t x_t + B_t u_t + d_t \\ & 0 \leq \varepsilon_t \\ & \tilde{C}_{s,t} x_t \leq \tilde{b}_{s,t} + \mathbf{1} \varepsilon_t \\ & u_t \in U_t \end{aligned} \quad (18)$$

which is similar to LP (17). In contrast to LP (17), an initial violation of the tightened state constraints is assumed (i.e.,  $x_0 \notin \tilde{G}_0$ ) and the inequality constraints  $\varepsilon_{t-1} \leq \varepsilon_t$  are removed in LP (18). Thus, the control associated with LP (18) tries to steer the state vector back into the set  $\tilde{G}_t$  (i.e., it tries to satisfy  $\tilde{C}_{s,t} x_t \leq \tilde{b}_{s,t}$ ) over the time horizon  $N_{\text{recover}}$ . Hence, the control computation based on  $\tilde{G}_t$ , as well as the recovery controller may prevent premature violation of the original constraints ( $x_t \notin G_t$ ), as illustrated in the bottom of Fig. 1.

The MPC strategy is outlined in Algorithm 2. At each time instant  $t_{\text{sys}}$ , the current state vector  $x(t_{\text{sys}})$  is acquired and used as the initial  $x_0$  for control computation (step 4 of Algorithm 2). The time-dependent dynamics and constraints for the linear DCOC problem [Eq. (16)] are obtained in step 3 based on the current time instant  $t_{\text{sys}}$  of the system for  $t \in \{0, 1, \dots, N_{\text{ub}} + N_{\text{add}}\}$ , where  $N_{\text{ub}} + N_{\text{add}}$  is the largest possible time horizon for LP (17) and  $N_{\text{recover}} \ll N_{\text{ub}}$  is used for the time horizon of LP (18). The parameter  $N_{\text{ub}}$  is defined in the following. If the tightened state constraints are not satisfied by the current state vector, the recovery controller is employed in step 6 of Algorithm 2. Otherwise, in combination with a modified version of Algorithm 1, LP (17) is used for control computation.

In contrast to previously proposed MPC schemes [11,12], the iterative procedure in Algorithm 1 is modified for the MPC scheme by including an upper bound  $N_{\text{ub}}$  on the time horizon  $N$  (step 15 of Algorithm 2). This allows premature termination of the iteration if, for example, computation time limits need to be satisfied. However, the optimal first exit time corresponding to the current state vector may be greater than  $N_{\text{ub}}$ , which may lower the quality of the resulting

solution. In addition to  $N_{\text{ub}}$ , the variable  $\tau_{\text{lb},0}$  is introduced to initialize the lower bound  $\tau_{\text{lb}}$  for LP (17) in step 8, in which  $\tau_{\text{lb},0}$  is updated over the receding time horizon in step 18 based on the first exit time of the previously computed solution. This significantly reduces the number of decision variables  $\varepsilon_t$  of LP (17) and decreases computation times. However, steps 10–12 need to be added to check if LP (17) is feasible for the current  $\tau_{\text{lb}}$  and  $N$ . This is important because, at time instant  $t_{\text{sys}} + 1$ , the predicted  $\tau_{\text{lb}}$  may be greater than the actual optimal first exit time for  $x_0 = x(t_{\text{sys}} + 1)$  as a consequence of prediction errors caused by unmodeled effects not present in the linear model. In this case, LP (17) becomes infeasible. Feasibility is recovered by recomputing  $\tau_{\text{lb}}$  in step 11 using the zero-control solution  $\tilde{\tau}(x_0, \{0\})$ , assuming  $0 \in U_t$  (otherwise, any admissible control sequence can be used).

## IV. Numerical Case Studies

The numerical results for two DCOC problems of GEO satellite station keeping (Sec. IV.A) and spacecraft attitude control (Sec. IV.B) are presented in this section. Although the proposed DCOC framework allows the treatment of time-dependent state and control constraints, time-invariant constraints are assumed in both problems ( $G_t \equiv G$  and  $U_t \equiv U$ ). Similarly,  $A_t \equiv A$  and  $B_t \equiv B$  in both problems.

To illustrate the conclusions from the analysis in a setting consistent with the assumptions in this paper, the open-loop solution of NLP (13) is compared to the LP-based MPC strategy (Algorithm 2) simulated on the discrete-time nonlinear model, which is on the model consistent with our design assumptions (i.e., discrete-time dynamics). To provide more realistic results (all systems evolve in continuous time in the real world), the MPC strategy is also simulated on the corresponding continuous-time nonlinear model using a zero-order hold for the control input. Hence, the following three simulation scenarios are considered in this section: 1) *NLP-Discrete-Time*, in which the open-loop solution of NLP (13) is simulated on the discrete-time nonlinear model; 2) *MPC-Discrete-Time*, in which the MPC strategy (Algorithm 2) is simulated in a closed loop with the discrete-time nonlinear model; and 3) *MPC-Continuous-Time*, in which the MPC strategy (Algorithm 2) is simulated in a closed loop with the continuous-time nonlinear model with a zero-order hold applied to the control input during each sampling period.

All computations in this section are performed in MATLAB 2015a on a laptop with an i5-6300 processor and 8 GB of RAM, in which the LPs are solved using the Hybrid Toolbox [31]. A solution to NLP (13) is obtained with the MATLAB function `fmincon`, for which the time horizon  $N$  and the lower bound  $\tau_{\text{lb}}$  are chosen based on the open-loop solution to the linear DCOC problem obtained by Algorithm 1 (using a small  $N_{\text{add}}$  of five). If the NLP solution does not violate the prescribed constraints for this parameter setting,  $N$  and  $\tau_{\text{lb}}$  are updated in analogy to Algorithm 1 (using a small  $N_{\text{add}}$  of five); then, the corresponding NLP is solved, and the procedure is repeated until constraint violation occurs. Based on Remark 1, this ensures that the first exit time of the NLP solution is close to the optimal first exit time of problem (5).

### A. GEO Satellite Station Keeping

#### 1. Nonlinear Model

Let frame  $\mathcal{I}$  be the Earth-centered inertial (ECI) frame and frame  $\mathcal{H}$  be Hill's frame. The 1-axis of Hill's frame is pointing radially from the center of the Earth to the current position on the reference orbit (i.e., along  $\mathbf{r}_{\text{GEO}/E}$ ), and the 2-axis points in the orbital track direction of the GEO reference orbit. The 3-axis completes the right-hand rule, pointing out of the equatorial plane in the GEO case. We denote the spacecraft position vector relative to the GEO reference orbit, resolved in Hill's frame, by  $\mathbf{r}_{\text{SC}/\text{GEO}}|_{\mathcal{H}} = \bar{\mathbf{r}}_{\text{SC}/\text{GEO}} = [r_1, r_2, r_3]^T$ . Similarly, the spacecraft velocity relative to the reference orbit with respect to Hill's frame, resolved in Hill's frame, is  $\bar{\mathbf{v}}_{\text{SC}/\text{GEO}}|_{\mathcal{H}} = [v_1, v_2, v_3]^T$ . The discrete-time nonlinear model that we consider to describe the spacecraft motion relative to the GEO reference orbit is obtained from the continuous-time nonlinear model, derived in Appendix A, using Euler's forward method and yielding

#### Algorithm 2 LP-based MPC implementation

---

```

1:  $t_{\text{sys}} \leftarrow 0$ 
2:  $\tau_{\text{lb},0} \leftarrow$  set initial lower bound
3:  $A_t, B_t, d_t, \tilde{G}_t, U_t \leftarrow$  obtain dynamics and constraints for all
    $t \in \{0, 1, \dots, N_{\text{ub}} + N_{\text{add}}\}$ 
4:  $x_0 \leftarrow$  current state  $x(t_{\text{sys}})$ 
5: if  $x_0 \notin \tilde{G}_0$ , then
6:    $\{u_t\} \leftarrow$  solution of LP (18)
7: else
8:    $\tau_{\text{lb}} \leftarrow \tau_{\text{lb},0}$ 
9:    $N \leftarrow \tau_{\text{lb}} + N_{\text{add}}$ 
10:  if LP (17) is infeasible, then
11:     $\tau_{\text{lb}} \leftarrow \min\{\tilde{\tau}(x_0, \{0\}), N_{\text{ub}}\}$ ; go to step 9
12:  end if
13:   $\{u_t\}, \{\varepsilon_{\tau_{\text{lb}}}, \dots, \varepsilon_N\} \leftarrow$  solution of LP (17)
14:   $\tau \leftarrow \max\{t \leq N: \varepsilon_t = 0\} + 1$ 
15:  if  $\varepsilon_N = 0$  and  $N < N_{\text{ub}}$ , then
16:     $\tau_{\text{lb}} \leftarrow \tau$ ; go to step 9
17:  end if
18:   $\tau_{\text{lb},0} \leftarrow \min\{\tau - 1, N_{\text{ub}}\}$ 
19: end if
20: Apply  $u_0$  as control input  $u(t_{\text{sys}})$  to the system
21:  $t_{\text{sys}} \leftarrow t_{\text{sys}} + 1$ ; go to step 3

```

---

$$\begin{bmatrix} \bar{r}_{SC/GEO,t+1} \\ \bar{v}_{SC/GEO/\mathcal{H},t+1} \end{bmatrix} = \begin{bmatrix} \bar{r}_{SC/GEO,t} \\ \bar{v}_{SC/GEO/\mathcal{H},t} \end{bmatrix} + \Delta t \begin{bmatrix} \bar{v}_{SC/GEO/\mathcal{H},t} \\ \bar{a}_{SC/GEO/\mathcal{H},t} \end{bmatrix} \quad (19)$$

where  $\bar{a}_{SC/GEO/\mathcal{H},t} = [a_{1,t}, a_{2,t}, a_{3,t}]^T$  and, using  $r_t = \sqrt{(r_{1,t} + r_0)^2 + r_{2,t}^2 + r_{3,t}^2}$ ,

$$\begin{aligned} a_{1,t} &= -\frac{\mu_E(r_{1,t} + r_0)}{r_t^3} + 2n_0v_{2,t} + n_0^2r_{1,t} + \frac{\mu_E}{r_0^2} + \frac{F_{1,t}}{m_{SC}} + d_{p,1,t}, \\ a_{2,t} &= -\frac{\mu_E r_{2,t}}{r_t^3} - 2n_0v_{1,t} + n_0^2r_{2,t} + \frac{F_{2,t}}{m_{SC}} + d_{p,2,t}, \\ a_{3,t} &= -\frac{\mu_E r_{3,t}}{r_t^3} + \frac{F_{3,t}}{m_{SC}} + d_{p,3,t} \end{aligned} \quad (20)$$

*Remark 2:* In this paper, Euler's forward method is used for discretization, which is sufficient for the purposes of this paper, i.e., comparing the MPC solution to the NLP solution (MPC-Discrete-Time versus NLP-Discrete-Time). The accuracy of the discretized model can be improved by using higher-order discretization schemes such as 4th order Runge–Kutta (RK4). At the same time, the use of Euler discretization yields simpler discrete-time models for MPC development, whereas the use of MPC with the solution being recomputed provides a form of feedback that compensates for discretization errors.

The control variables  $F_1$ ,  $F_2$ , and  $F_3$  are the thrust forces along the unit (i.e., projected on the axes) of Hill's frame:

$$u = \bar{F} = [F_1, F_2, F_3]^T \quad (21)$$

Likewise,  $d_{p,1}$ ,  $d_{p,2}$ , and  $d_{p,3}$  are perturbations projected on the axes of Hill's frame according to Eqs. (A7–A11) in which, in this paper, we take into account perturbations due to lunisolar gravity, SRP, and  $J_2$ . Note that additional perturbations can readily be included, which is not done here because the results are compared to [19], in which a satellite model with the aforementioned perturbations was considered. The trajectories of Earth, moon, and sun are obtained from the Jet Propulsion Laboratory's HORIZONS Web interface [32] in which, in all simulations, the initial positions were as of 3 September 2015 at 1200 hrs Central Time (CT).

The other parameters in Eq. (19) are the spacecraft mass  $m_{SC}$ , Earth's gravitational parameter  $\mu_E$ , the GEO radius of  $r_0 = 42,160$  km, and the GEO angular rate  $n_0$ ; see Eq. (A4). Because the fuel mass is assumed to be much smaller than  $m_{SC}$ ,  $m_{SC}$  is considered constant.

In addition to the six states in Eq. (19), another state is introduced that takes account of the available fuel. To normalize fuel consumption, we use the accumulated  $\Delta v$  (total change in spacecraft velocity) due to accelerations generated by the thrust forces. Thus,

$$\Delta v_{acc,t+1} = \Delta v_{acc,t} + \Delta v_t = \Delta v_{acc,t} + \Delta t \frac{\|u_t\|_1}{m_{SC}} \quad (22)$$

where  $\|\cdot\|_1$  denotes the 1-norm.

In summary, the discrete-time nonlinear spacecraft model for problem (5) is given by Eqs. (19) and (22), where the control input and state vector, respectively, are given by Eq. (21) and  $x = [r_1, r_2, r_3, v_1, v_2, v_3, \Delta v_{acc}]^T$ .

## 2. DCOC Problem

Consider a station-keeping window of  $\pm 0.01^\circ$  in longitude and latitude, which is an order of magnitude smaller as compared to traditional station-keeping approaches [14,16,17]. Note that future missions may require such small windows due to the growing number of GEO satellites. The chosen constraints on longitude and latitude approximately translate into position constraints of  $\pm 7.4$  km for  $r_1$ ,  $r_2$ , and  $r_3$ . Hence, the set defining the state constraints for problem (5) is given by

$$G = \{x \in \mathbb{R}^7 : \Delta v_{acc} \in [0, \Delta v_{acc,max}], r_i \in [-7.4, 7.4] \text{ km}, i \in \{1, 2, 3\}\} \quad (23)$$

where  $\Delta v_{acc,max}$  is a prescribed maximum value for the accumulated  $\Delta v$ , which is equivalent to the amount of fuel that is initially available. The control objective is to maximize the time that the state vector remains inside  $G$ . The tightened constraints  $\tilde{G}_t \equiv \tilde{G}$  for the MPC implementation [see Fig. 1 and Eq. (14)] are obtained by reducing the position window by 0.1%, yielding

$$\tilde{G} = \{x \in \mathbb{R}^7 : \Delta v_{acc} \in [0, \Delta v_{acc,max}], r_i \in [-7.3926, 7.3926] \text{ km}, i \in \{1, 2, 3\}\} \quad (24)$$

The satellite is equipped with six thrusters, for which each thruster can generate a maximum thrust force of  $F_{th} = 0.1$  N, which is similar to the ion thruster discussed in [33]. Each thruster is assumed to point in one of the directions of Hill's frame (positive and negative directions). Assuming continuous-thrust values, the control constraints are given by

$$U = \{[F_1, F_2, F_3]^T : F_i \in [-F_{th}, F_{th}], i \in \{1, 2, 3\}\}$$

A spacecraft mass of  $m_{SC} = 4000$  kg is assumed, and the parameters for the SRP disturbance model in Eq. (A10) are  $C_{srp} = 9.1 \times 10^{-6}$  N/m<sup>2</sup>,  $c_{refl} = 0.6$ , and  $S_{SC} = 200$  m<sup>2</sup>.

## 3. Linear Model

The linear discrete-time model for the MPC implementation is obtained by linearizing the continuous-time nonlinear model in Eq. (A6) about the GEO reference orbit, yielding the Clohessy–Wiltshire (CW) equations [34], and by employing Euler's forward method to transform the continuous-time model into discrete time. Furthermore, the nonlinear evolution of the accumulated  $\Delta v$  in Eq. (22) is approximated by introducing the auxiliary variables  $\zeta = [\zeta_1, \zeta_2, \zeta_3]^T$  and augmenting the linear discrete-time dynamics in Eq. (16) as follows:

$$x_{t+1} = Ax_t + B \begin{bmatrix} u_t \\ \zeta_t \end{bmatrix} + d_t \quad (25)$$

where matrices  $A$  and  $B$  are given in the following. Moreover, the constraints

$$-\zeta_t \leq u_t \leq \zeta_t, \quad t \in \{0, \dots, N-1\} \quad (26)$$

are added to LPs (17) and (18), and the weighted sum of  $\zeta_t$  is added to the respective objective function in order to approximate the nonlinear dynamics of  $\Delta v_{acc}$ . In this regard, the objective functions of LPs (17) and (18), respectively, are modified to

$$\sum_{t=\tau_{ib}}^N \varepsilon_t + w \sum_{t=0}^{N-1} \mathbf{1}^T \zeta_t \quad (27a)$$

$$\sum_{t=1}^{N_{\text{recover}}} \varepsilon_t + w \sum_{t=0}^{N_{\text{recover}}-1} \mathbf{1}^T \zeta_t \quad (27b)$$

where  $w > 0$  is a weight that is set to  $w = 0.005$ . The matrices of the linear discrete-time model in Eq. (25) are as follows:

$$A = \begin{bmatrix} 1 & 0 & 0 & \Delta t & 0 & 0 & 0 \\ 0 & 1 & 0 & 0 & \Delta t & 0 & 0 \\ 0 & 0 & 1 & 0 & 0 & \Delta t & 0 \\ 3n_0^2\Delta t & 0 & 0 & 1 & 2n_0\Delta t & 0 & 0 \\ 0 & 0 & 0 & -2n_0\Delta t & 1 & 0 & 0 \\ 0 & 0 & -n_0^2\Delta t & 0 & 0 & 1 & 0 \\ 0 & 0 & 0 & 0 & 0 & 0 & 1 \end{bmatrix} \quad (28)$$

$$B = \begin{bmatrix} 0_{3 \times 6} \\ \frac{\Delta t}{m_{SC}} & 0 & 0 & 0 & 0 & 0 \\ 0 & \frac{\Delta t}{m_{SC}} & 0 & 0 & 0 & 0 \\ 0 & 0 & \frac{\Delta t}{m_{SC}} & 0 & 0 & 0 \\ 0 & 0 & 0 & \frac{\Delta t}{m_{SC}} & \frac{\Delta t}{m_{SC}} & \frac{\Delta t}{m_{SC}} \end{bmatrix} \quad (29)$$

where  $n_0$  is defined in Eq. (A4), and  $\Delta t = 500$  s is the sampling time for the discrete-time transformation.

Following [19,35], the time-varying disturbance term  $d_t$  of the linear model given by Eq. (25) is computed in advance for the known GEO reference orbit by using Eqs. (A7–A11) with  $\mathbf{r}_{M/GEO}$ ,  $\mathbf{r}_{S/GEO}$ , and  $\mathbf{r}_{GEO/E}$  replacing  $\mathbf{r}_{M/SC}$ ,  $\mathbf{r}_{S/SC}$ , and  $\mathbf{r}_{SC/E}$ , respectively, where, instead of the spacecraft position (SC), the known position of the GEO reference orbit is used. Thus, the disturbing accelerations for the GEO reference orbit are obtained at each time instant and  $d_t$  follows from multiplying these accelerations by the sampling time  $\Delta t$  (Euler's forward method). Hence,  $d_t = [0_{1 \times 3}, \Delta t \bar{d}_{p,t}^T, 0]^T$ , with  $\bar{d}_{p,t}$  denoting the instantaneous disturbance vector for the GEO reference orbit, resolved in Hill's frame, according to Eq. (A7).

#### 4. Results

The following initial condition is considered:

$$x_0 = [0, 0, -5 \text{ km}, 0, -0.4 \text{ m/s}, 0, 0]^T \quad (30)$$

and the maximum value for the accumulated  $\Delta v$  in Eq. (23) is chosen as 1 m/s. The sampling time is set to  $\Delta t = 500$  s (for both the NLP and MPC approaches). Note that the initial condition in Eq. (30) and  $\Delta v_{\text{acc,max}} = 1$  m/s are chosen to ensure a sufficiently small time horizon for this problem to address computational feasibility in solving the NLP with `fmincon` in MATLAB. However, the chosen values also reflect a realistic objective to maximize the GEO satellite operational life near the end of its mission. The numerical treatment of larger time horizons is left for future work.

Regarding the MPC approach, the upper bound  $N_{\text{ub}}$  on the time horizon  $N$  of LP (17) in Algorithm 2 is set to 600 to ensure reasonable computation times in MATLAB because an initial numerical study over 1000 randomly generated  $x_0 \in G$  showed average and worst-case computation times for solving LP (17) of 4.3 and 18.5 s, respectively, when  $N = 600$  and  $\tau_{\text{lb}} = 1$ . The other parameters are set to  $N_{\text{add}} = 30$ ,  $N_{\text{recover}} = 5$ , and  $\tau_{\text{lb},0} = 300$  as an initial guess in step 2 of Algorithm 2.

The results of the NLP-Discrete-Time and MPC-Discrete-Time simulations are plotted in Fig. 2, in which the dashed lines indicate the state and control constraints. Figure 2 also shows the results of the MPC-Continuous-Time simulation (the continuous-time nonlinear model is derived in Appendix A). A constraint violation occurs as a consequence of reaching the prescribed fuel limit or, equivalently, the limit on  $\Delta v_{\text{acc}}$ . The trajectories for NLP-Discrete-Time and MPC-Discrete-Time simulations in Fig. 2 are similar, and the constraint violation occurs after 415 time steps (2.4 days) for both approaches. This shows that the LP-based MPC scheme can be effective in the context of DCOC of a nonlinear system. Applying the MPC strategy to the continuous-time nonlinear model results in control trajectories similar to the MPC-Discrete-Time solution. However, the continuous-time dynamics extend the constraint violation to 2.92 days, which is about 22% greater than observed in simulations on the discrete-time model, which may be due to the Euler forward discretization scheme (see Remark 2) and the relatively large sampling time of  $\Delta t = 500$  s of the discrete-time dynamics.

The computation times are as follows. About 53 min are required to solve NLP (13) with the MATLAB function `fmincon`. In both MPC-Discrete-Time and MPC-Continuous-Time simulations, the MPC strategy requires, on average, 1.4 s to compute the control input

at each time instant with a worst-case computation time of 16 s (which is smaller than  $\Delta t = 500$  s).

## B. Spacecraft Attitude Control

### 1. Nonlinear Model

The continuous-time nonlinear model for spacecraft attitude dynamics is summarized in Appendix B. Euler's forward method is used to obtain the discrete-time model from the continuous-time model for a chosen sampling time of  $\Delta t = 2$  s. The state vector at a time instant  $t \in \mathbb{Z}_{\geq 0}$  is given by

$$x_t = [\phi_t, \theta_t, \psi_t, \omega_{1,t}, \omega_{2,t}, \omega_{3,t}, \nu_{1,t}, \dots, \nu_{p,t}]^T$$

where  $\phi_t$ ,  $\theta_t$ , and  $\psi_t$  are the 3-2-1 Euler angles;  $\bar{\omega}_{B/\mathcal{I},t} = [\omega_{1,t}, \omega_{2,t}, \omega_{3,t}]^T$  is the spacecraft angular velocity vector (angular velocity of the spacecraft body-fixed frame  $\mathcal{B}$  relative to an inertial reference frame  $\mathcal{I}$ ) expressed in the body-fixed frame; and  $\bar{\nu}_t = [\nu_{1,t}, \dots, \nu_{p,t}]^T$  contains the spin rates of the  $p$  RWs. The RW accelerations serve as control variables, and the control input vector for the discrete-time model is given by the instantaneous RW accelerations, i.e.,  $u_t = [\dot{\nu}_{1,t}, \dots, \dot{\nu}_{p,t}]^T$ . Thus, the discrete-time nonlinear model is as follows:

$$\begin{bmatrix} \phi_{t+1} \\ \theta_{t+1} \\ \psi_{t+1} \\ \bar{\omega}_{B/\mathcal{I},t+1} \\ \bar{\nu}_{t+1} \end{bmatrix} = \begin{bmatrix} \phi_t \\ \theta_t \\ \psi_t \\ \bar{\omega}_{B/\mathcal{I},t} \\ \bar{\nu}_t \end{bmatrix} + \Delta t \begin{bmatrix} 1 & s(\phi_t)t(\theta_t) & c(\phi_t)t(\theta_t) \\ 0 & c(\phi_t) & -s(\phi_t) \\ 0 & s(\phi_t)/c(\theta_t) & c(\phi_t)/c(\theta_t) \end{bmatrix} \bar{\alpha}_{B/\mathcal{I},t} \begin{bmatrix} \bar{\omega}_{B/\mathcal{I},t} \\ u_t \end{bmatrix} \quad (31)$$

where  $c(\cdot) = \cos(\cdot)$ ,  $s(\cdot) = \sin(\cdot)$ ,  $t(\cdot) = \tan(\cdot)$ , and  $\bar{\alpha}_{B/\mathcal{I},t} = \bar{\omega}_{B/\mathcal{I},t}$  according to Eq. (B5); i.e.,

$$\bar{\alpha}_{B/\mathcal{I},t} = \bar{J}^{-1}(\bar{\tau}_{\text{srp},t} - S[\bar{\omega}_{B/\mathcal{I},t}](\bar{J}\bar{\omega}_{B/\mathcal{I},t} + J_w W \bar{\nu}_t) - J_w W u_t) \quad (32)$$

The SRP disturbance torque  $\bar{\tau}_{\text{srp}}$  in Eq. (32) is a nonlinear function of the spacecraft orientation; see Eqs. (B6–B7). The other parameters of the model are the moment of the inertia matrix of the spacecraft bus  $J$ , the moment of inertia of each RW (assuming identical RWs) about its spin axis  $J_w$ , and the locked inertia  $\bar{J}$  [see Eq. (B4)], as well as the orientations of the RW spin axes given by  $W$  [see Eq. (B3)]. We consider a spacecraft with the parameters listed in Table 1. Note that the vector representing the direction of the sun is resolved in the inertial frame  $\mathcal{I}$  in Table 1 and needs to be transformed into the spacecraft body-fixed frame  $\mathcal{B}$  continuously using the current orientation of the spacecraft.

### 2. DCOC Problem

The objective is to satisfy the prescribed constraints on spacecraft orientation and the RW spin rates for as long as possible. The constraints define the set

$$G = \{x \in \mathbb{R}^{6+p} : \phi \in [\phi_{\min}, \phi_{\max}], \theta \in [\theta_{\min}, \theta_{\max}], \psi \in [\psi_{\min}, \psi_{\max}], \nu_i \in [\nu_{i,\min}, \nu_{i,\max}], i \in \{1, 2, \dots, p\}\} \quad (33)$$

where  $\phi_{\min} < 0$ ,  $\theta_{\min} < 0$ ,  $\psi_{\min} < 0$ ,  $\phi_{\max} > 0$ ,  $\theta_{\max} > 0$ ,  $\psi_{\max} > 0$ , and  $\nu_{i,\min} < \nu_{i,\max} \in \mathbb{R}$ ,  $i \in \{1, 2, \dots, p\}$ . Similar to the GEO station-keeping problem in Sec. IV.A, as illustrated in Fig. 1, we tighten the state constraints for the LP-based MPC implementation

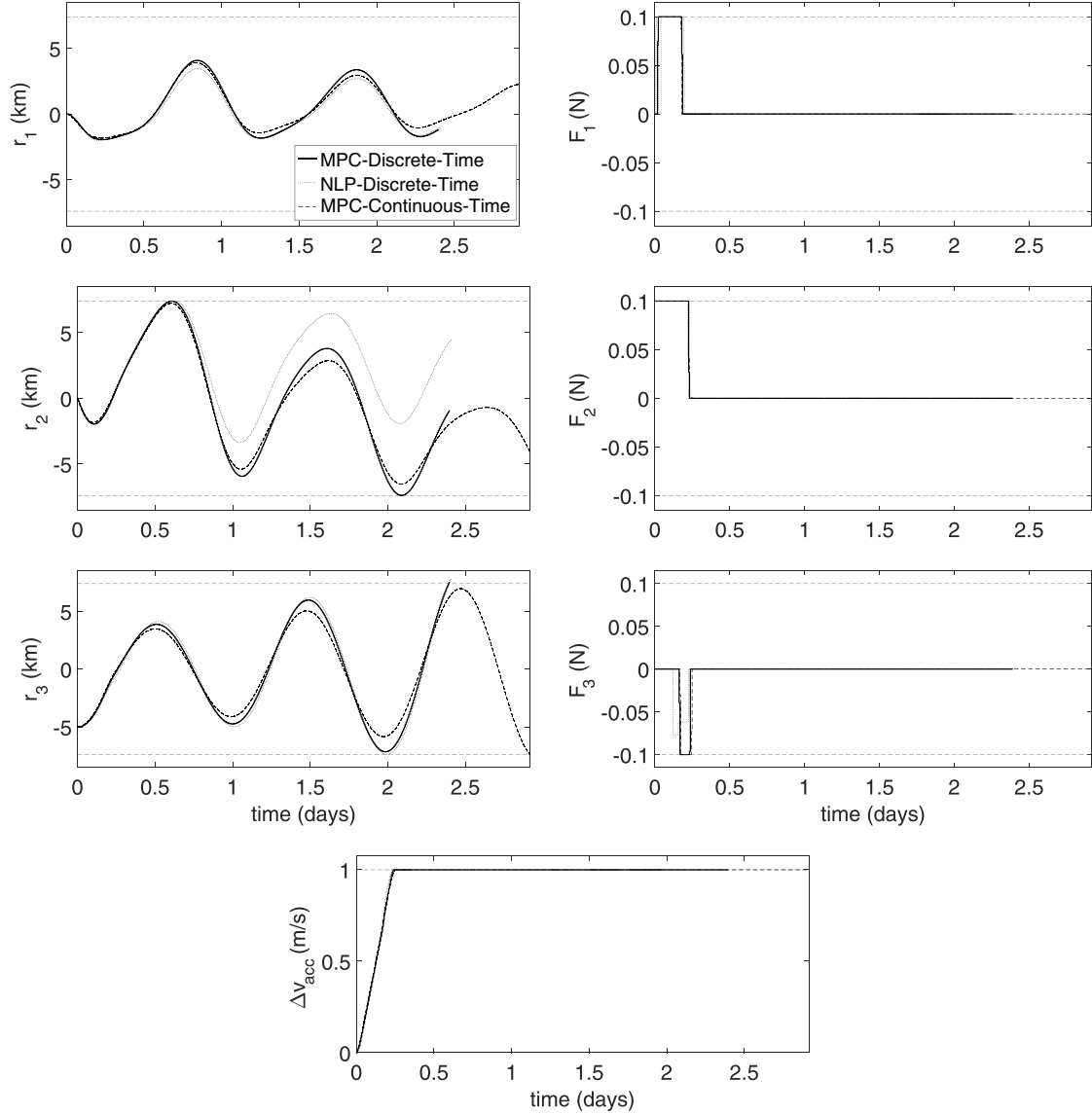


Fig. 2 GEO satellite station-keeping problem with  $\Delta v_{\text{acc,max}} = 1$  m/s and  $x_0$  in Eq. (30): spacecraft position relative to GEO reference orbit,  $r_{\text{SC}/\text{GEO}}|_{\mathcal{H}} = [r_1, r_2, r_3]^T$ , and thrust forces  $F|_{\mathcal{H}} = [F_1, F_2, F_3]^T$  resolved in Hill’s frame, as well as accumulated  $\Delta v$  vs time.

by reducing the orientation constraints by 0.4%, which yields the reduced set

$$\tilde{G} = \{x \in \mathbb{R}^{6+p} : 1.004\phi \in [\phi_{\min}, \phi_{\max}], 1.004\theta \in [\theta_{\min}, \theta_{\max}], 1.004\psi \in [\psi_{\min}, \psi_{\max}], \nu_i \in [\nu_{i,\min}, \nu_{i,\max}], i \in \{1, 2, \dots, p\}\} \quad (34)$$

In the following case studies (Secs. IV.B.4–IV.B.6), the attitude and RW spin rate constraints in Eqs. (33) and (34), respectively, are given by

$$\phi_{\min} = \theta_{\min} = -0.00175 \text{ rad}, \quad \psi_{\min} = -0.0175 \text{ rad} \quad (35a)$$

$$\phi_{\max} = \theta_{\max} = 0.00175 \text{ rad}, \quad \psi_{\max} = 0.0175 \text{ rad} \quad (35b)$$

$$\nu_{i,\min} = 10 \text{ rad/s}, \quad \nu_{i,\max} = 250 \text{ rad/s}, \quad i \in \{1, 2, \dots, p\} \quad (35c)$$

Note that the lower bound on the RW spin rates is chosen to avoid zero speed crossings and increase in RW wear and power consumption at low speeds. The initial states of the spacecraft are assumed to be

$$[\phi_0, \theta_0, \psi_0] = [-0.001, 0.00035, -0.0105] \text{ rad} \quad (36a)$$

$$[\omega_{1,0}, \omega_{2,0}, \omega_{3,0}] = [3.5, 3.5, 35] \times 10^{-5} \text{ rad/s} \quad (36b)$$

The maximum angular acceleration of each RW is  $4 \text{ rad/s}^2$ . Hence,

Table 1 Model parameters for spacecraft attitude control problem [26]

Parameter	Units	Value
$J$	kg/m <sup>2</sup>	diag(430, 1210, 1300)
$J_w$	kg/m <sup>2</sup>	0.043
$L_x, L_y, L_z$	m	2, 2.5, 5
$l_x, l_y, l_z$	m	0, 0.5, 0
$\hat{q}_S _{\mathcal{I}}$	---	$[0, 1/\sqrt{2}, 1/\sqrt{2}]^T$
$\Phi_S$	W/m <sup>2</sup>	1367
$c$	m/s	299, 792, 458
$C_{\text{diff}}$	---	0.2

$$U = \{u \in \mathbb{R}^p: u_i \in [-4, 4] \text{ rad/s}^2, i \in \{1, 2, \dots, p\}\} \quad (37)$$

### 3. Linear Model

In analogy to the previous case study (Sec. IV.A), the linear discrete-time model for the LP-based MPC implementation (Algorithm 2) is obtained by linearizing the continuous-time nonlinear model (Appendix B) and employing Euler's forward method using a sampling time of  $\Delta t = 2$  s. We choose  $\phi = \theta = \psi = 0$  and the initial RW spin rates  $\bar{v}_0$  as the reference for the linear model. The matrices and the disturbance term of the linear discrete-time model are therefore given by

$$A = \begin{bmatrix} I_{3 \times 3} & \Delta t I_{3 \times 3} & 0_{3 \times p} \\ \Delta t \bar{J}^{-1} T & I_{3 \times 3} + \Delta t \bar{J}^{-1} J_w S[W \bar{v}_0] & 0_{3 \times p} \\ 0_{p \times 3} & 0_{p \times 3} & I_{p \times p} \end{bmatrix} \quad (38)$$

$$B = \begin{bmatrix} 0_{3 \times p} \\ -\Delta t \bar{J}^{-1} J_w W \\ \Delta t I_{p \times p} \end{bmatrix}, \quad d = \begin{bmatrix} 0_{3 \times 1} \\ \Delta t \bar{J}^{-1} \bar{\tau}_{\text{srp}}|_{\phi=\theta=\psi=0} \\ 0_{p \times 1} \end{bmatrix} \quad (39)$$

where  $S[\cdot]$  is the skew-symmetric matrix defined in Eq. (B1), and  $\bar{\tau}_{\text{srp}}|_{\phi=\theta=\psi=0}$  is the SRP torque when  $\phi = \theta = \psi = 0$ . Furthermore,  $T$  in Eq. (38) results from numerically linearizing the SRP torque in Eq. (B7) about  $\phi = \theta = \psi = 0$ , i.e.,

$$\bar{\tau}_{\text{srp}} \approx \bar{\tau}_{\text{srp}}|_{\phi=\theta=\psi=0} + T[\phi, \theta, \psi]^T$$

Note that the disturbance term in Eq. (39) is time invariant in this example due to the assumption of constant SRP.

Initial numerical results showed that, compared to the open-loop solutions, the LP-based MPC strategy (in MPC-Discrete-Time and MPC-Continuous-Time simulations) yields similar first exit times while, however, using substantially more control effort. This may be undesirable when considering onboard energy consumption/limited energy and RW component life. Hence, in order to avoid excessive control inputs, control inputs are penalized by considering the weighted sum of  $\|u_t\|_1$  values as an additional objective to be minimized. As, for example, in [36], this is achieved by introducing the variables  $\gamma_t \in \mathbb{R}^p$  for  $t \in \{0, 1, \dots, N-1\}$  and adding the weighted sum of  $\gamma_t$  values to the objective functions of LPs (17) and (18), yielding, respectively,

$$\sum_{t=\tau_{\text{lb}}}^N \varepsilon_t + w \sum_{t=0}^{N-1} \mathbf{1}^T \gamma_t \quad \text{and} \quad \sum_{t=1}^{N_{\text{recover}}} \varepsilon_t + w \sum_{t=0}^{N_{\text{recover}}-1} \mathbf{1}^T \gamma_t \quad (40)$$

where the weight is set to  $w = 0.005$  here. Moreover, the constraints  $-\gamma_t \leq u_t \leq \gamma_t, t \in \{0, 1, \dots, N-1\}$ , are added to LPs (17) and (18). This approach is similar to the linear approximation of the nonlinear dynamics of  $\Delta v_{\text{acc}}$  in the GEO satellite station-keeping problem; see Eqs. (22), (26), and (27).

In the following, we use  $N_{\text{ub}} = 200$ ,  $N_{\text{add}} = 25$ ,  $N_{\text{recover}} = 5$ , and  $\tau_{\text{lb},0} = 100$  (initial guess) for the MPC implementation in Algorithm 2.

### 4. Results for One RW

First, the case of one operable RW ( $p = 1$ ) with a spin axis of  $\bar{g}_1 = [1/\sqrt{3}, 1/\sqrt{3}, 1/\sqrt{3}]^T$  (resolved in the spacecraft body-fixed frame) is considered. The set of state constraints and the initial condition of the spacecraft for this case study are given by Eqs. (35) and (36), respectively; and the initial RW speed is assumed to be  $\bar{v}_0 = 100$  rad/s. Figure 3 shows the trajectories of the Euler angles, the RW speed, and the control input for the NLP-Discrete-Time and MPC-Discrete-Time simulations, as well as for the MPC-Continuous-Time

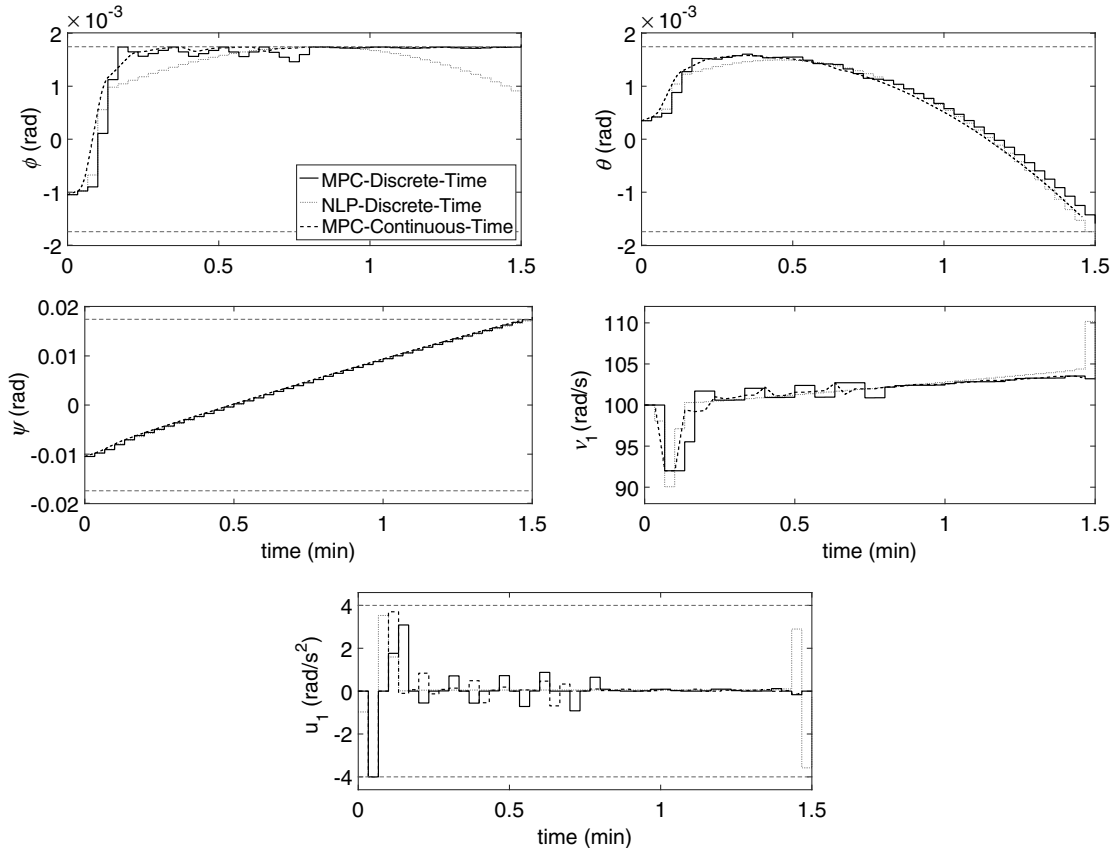


Fig. 3 Spacecraft attitude control problem, with one RW ( $p = 1$ ): Euler angles, RW speed, and control input vs time.

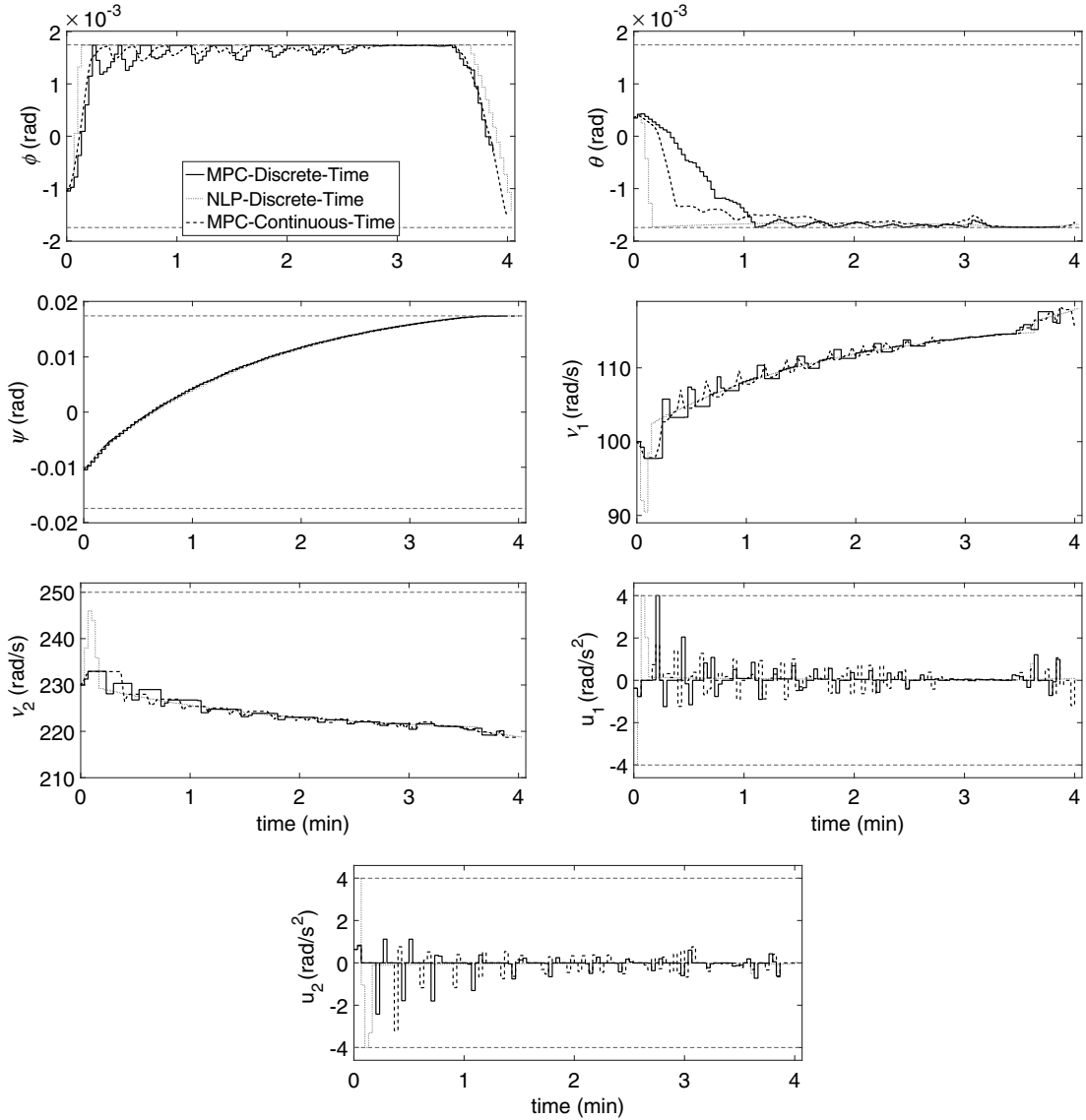


Fig. 4 Spacecraft attitude control problem, with two RWs ( $p = 2$ ): Euler angles, RW speeds, and control inputs vs time.

simulation (where a zero-order hold is applied to the control during each 2 s sampling interval). The constraints are indicated by gray dashed lines in Fig. 3. Both the NLP-Discrete-Time and MPC-Discrete-Time solutions violate the constraints after 45 time steps, which are equivalent to 90 s (1.5 min). The respective trajectories are similar but different, which indicates that the optimal solution to problem (5) may not be unique in this case.

In the MPC-Continuous-Time simulation, the constraint violation occurs after 87.4 s (1.46 min). The NLP solution is obtained in 49.9 s with MATLAB's `fmincon` function, which is considerably faster as compared to the GEO station-keeping problem (Sec. IV.A) because of smaller first exit times (and thus smaller time horizons). On average, the LP-based MPC implementation (in both MPC-Discrete-Time and MPC-Continuous-Time simulations) requires about 0.01 s to compute the control input at each time instant, and the worst-case computation time is 0.08 s.

##### 5. Results for Two RWs

Now, two operable RWs are assumed ( $p = 2$ ), which increases the spacecraft's control authority as compared to  $p = 1$ . In addition to the RW with a spin axis of  $\bar{g}_1 = [1/\sqrt{3}, 1/\sqrt{3}, 1/\sqrt{3}]^T$ , the spacecraft has a second RW with a spin axis of  $\bar{g}_2 = [0, 1, 0]^T$ . The initial RW spin rates are given by  $\bar{v}_0 = [100, 230]^T$  rad/s.

The responses based on the LP-based MPC strategy (in MPC-Discrete-Time and MPC-Continuous-Time simulations) as well as

the NLP solution (in the NLP-Discrete-Time simulation) for the state constraints and initial condition in Eqs. (35) and (36), respectively, are plotted in Fig. 4. The gray dashed lines in Fig. 4 indicate the prescribed constraints. As for the case of  $p = 1$ , the MPC solutions are close to the open-loop NLP solution. There are differences, however, because the MPC strategy exploits a linear model and control adjustments are required when the predicted trajectory differs from the actual trajectory due to unmodeled effects. The NLP solution violates constraints after 122 time steps or 244 s (4.1 min). Similarly, the MPC-Discrete-Time simulation shows a constraint violation after 117 time steps or 234 s (3.9 min). A constraint violation occurs after 240 s (4 min) in the MPC-Continuous-Time simulation. In the worst-case, the MPC implementation (in both MPC-Discrete-Time and MPC-Continuous-Time simulations) requires 0.22 s to compute the control  $u_i$  at a time instant  $t \in \mathbb{Z}_{\geq 0}$  and 0.05 s on average. The open-loop NLP solution, on the other hand, is computed in 136 s.

##### 6. Results for Three RWs

In the case of three operable RWs ( $p = 3$ ), the spacecraft is fully actuated. For this case study, a third RW with a spin axis of  $\bar{g}_3 = [0, 0, 1]^T$  is added to the two RWs with spin axes of  $\bar{g}_1 = [1/\sqrt{3}, 1/\sqrt{3}, 1/\sqrt{3}]^T$  and  $\bar{g}_2 = [0, 1, 0]^T$ . As before, the state constraints and initial condition are as in Eqs. (35) and (36), respectively; and the initial RW speeds of  $\bar{v}_0 = [100, 230, 249.7]^T$  rad/s are

assumed. Note that the third RW is initially near its saturation limit. Thus, the control authority is limited and, despite being fully actuated, the constraint violation occurs in finite time for any admissible control law.

The NLP solution violates constraints after 216 time steps or 432 s (7.2 min). For the MPC implementation, a constraint violation occurs after 209 time steps or 418 s (6.97 min) in the MPC discrete-time case and after 419.6 s (6.99 min) in the MPC-Continuous-Time case. These relatively large differences versus the NLP solution can be attributed to the weight  $w$  that emphasizes minimum control effort in LPs (17) and (18); see Eq. (40). The respective first exit times are improved by reducing  $w$  from 0.005 to 0.001. This change results in a constraint violation after 213 time steps or 424 s (7.07 min) in the MPC discrete-time simulation, which is within 1.5% of the NLP solution. Furthermore, with the modified weight, a constraint

violation occurs after 426.9 s (7.12 min) in the MPC-Continuous-Time simulation. Further reducing  $w$  does not significantly improve the first exit times. Figure 5 shows the trajectories of the NLP solution as well as of the MPC solutions (in MPC-Discrete-Time and MPC-Continuous-Time simulations) for  $w = 0.001$ .

A computation time of 461 s is required to obtain the NLP solution. For the LP-based MPC implementation, the worst-case time to compute the control is 1.12 s, and 0.14 s are required on average. Thus, for the cases considered (Secs. IV.B.4–IV.B.6), the worst-case computation times are below the sampling time of  $\Delta t = 2$  s. Computation times can be further reduced by increasing  $\Delta t$  and/or reducing the upper bound  $N_{ub}$  on the time horizon of LP (17) in Algorithm 2, which may, however, reduce the control performance (i.e., lead to earlier constraint violation).

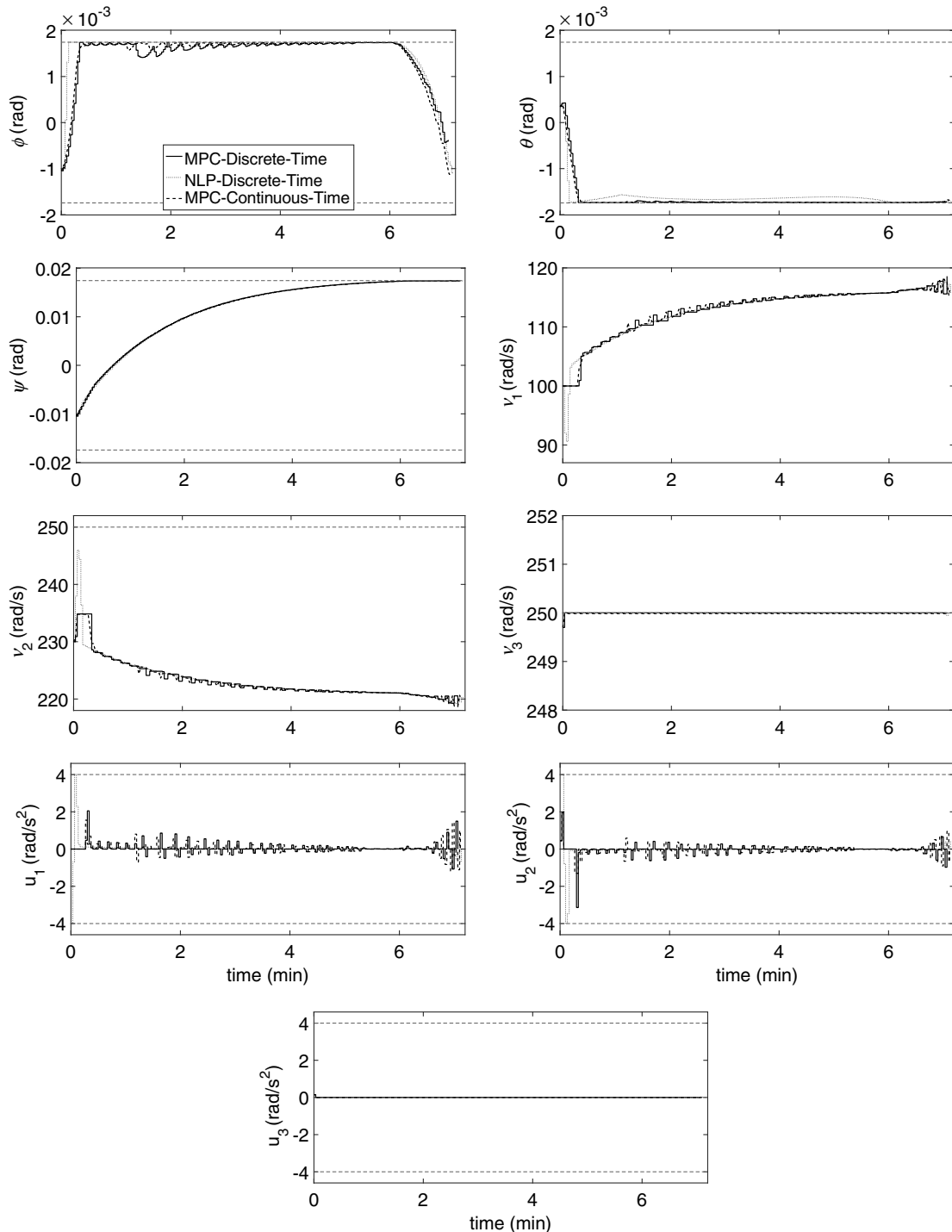


Fig. 5 Spacecraft attitude control example, with three RWs ( $p = 3$ ): Euler angles, RW speeds, and control inputs vss time.

## V. Conclusions

This paper treated an optimal control problem of maximizing the time before a system violates constraints. A mixed-integer nonlinear program was derived that led to an open-loop solution of the problem. A similar nonlinear program without integer variables was presented that provided good-quality suboptimal solutions. In addition, a model predictive control (MPC)-based closed-loop strategy was developed, based on a linear model approximation of the system and the application of standard linear programming. The resulting algorithmic procedures were applied to two challenging spacecraft control problems. In the first problem of GEO satellite station keeping, the objective was to satisfy prescribed orbital position constraints for as long as possible, given fuel limitations and orbital perturbations. In the second problem, a spacecraft with reaction wheels was considered and tight pointing constraints had to be satisfied for as long as possible, given solar radiation pressure disturbance torques and underactuation caused by RW failures or RWs close to saturation limits. In both cases, the developed MPC strategy successfully delayed the constraint violation and the MPC solutions were shown to provide similar performance to the nonlinear programming solutions. Future research will focus on efficiently handling problems with longer time horizons in a numerical setting: in particular, using the MPC approach. Additionally, there is room for future research on stochastic or robust versions of DCOC: for example, to address uncertainty in the prediction model.

### Appendix A: Nonlinear Model for GEO Satellite Station-Keeping Problem

The derivation of the nonlinear spacecraft model for the GEO station-keeping problem (Sec. IV.A) is described here. With frame  $\mathcal{I}$  as the ECI frame and frame  $\mathcal{H}$  as Hill's frame, a vector  $\mathbf{r}$  (resolved in frame  $\mathcal{I}$ ) is transformed into frame  $\mathcal{H}$  according to  $\mathbf{r}|_{\mathcal{H}} = \mathbf{O}_{\mathcal{H}/\mathcal{I}}\mathbf{r}|_{\mathcal{I}}$ , where  $\mathbf{O}_{\mathcal{H}/\mathcal{I}}$  is the respective orientation matrix. In the GEO case, and assuming that the initial true anomaly of the reference orbit is zero,  $\mathbf{O}_{\mathcal{H}/\mathcal{I}}$  is as follows:

$$\mathbf{O}_{\mathcal{H}/\mathcal{I}} = \begin{bmatrix} \cos(n_0 t) & \sin(n_0 t) & 0 \\ -\sin(n_0 t) & \cos(n_0 t) & 0 \\ 0 & 0 & 1 \end{bmatrix} \quad (\text{A1})$$

where  $n_0$  is defined in Eq. (A4). Likewise,  $\mathbf{r}|_{\mathcal{I}} = \mathbf{O}_{\mathcal{H}/\mathcal{I}}^T \mathbf{r}|_{\mathcal{H}} = \mathbf{O}_{\mathcal{I}/\mathcal{H}} \mathbf{r}|_{\mathcal{H}}$ . In the following, we use  $\bar{\mathbf{r}} = \mathbf{r}|_{\mathcal{H}}$  to denote a vector resolved in Hill's frame. Furthermore, the time derivative of a vector  $\mathbf{r}$  with respect to frame  $\mathcal{F}$  is denoted by  $\dot{\mathbf{r}}^{\mathcal{F}}$ . The spacecraft position vector relative to Earth's center is denoted by  $\mathbf{r}_{\text{SC}/E}$ , and the velocity and acceleration vectors with respect to frame  $\mathcal{I}$  are  $\mathbf{v}_{\text{SC}/E/\mathcal{I}} = \dot{\mathbf{r}}_{\text{SC}/E}^{\mathcal{I}}$  and  $\mathbf{a}_{\text{SC}/E/\mathcal{I}} = \ddot{\mathbf{r}}_{\text{SC}/E}^{\mathcal{I}}$ , respectively. Thus, employing the two-body problem in continuous time [34], we get

$$\mathbf{a}_{\text{SC}/E/\mathcal{I}} = -\frac{\mu_E}{\|\mathbf{r}_{\text{SC}/E}\|_2^3} \mathbf{r}_{\text{SC}/E} + \frac{\mathbf{F}}{m_{\text{SC}}} + \mathbf{d}_p \quad (\text{A2})$$

where  $\mu_E$  is Earth's gravitational parameter,  $\mathbf{F}$  denotes the thrust vector,  $m_{\text{SC}}$  is the spacecraft mass, and  $\mathbf{d}_p$  is a vector containing perturbing accelerations. Instead of Eq. (A2), we describe the spacecraft motion relative to a GEO reference orbit, i.e.,  $\mathbf{r}_{\text{SC}/\text{GEO}}$ . Hence, an expression for the relative acceleration vector with respect to Hill's frame  $\mathbf{a}_{\text{SC}/\text{GEO}/\mathcal{H}}$  needs to be derived. It is  $\mathbf{a}_{\text{SC}/\text{GEO}/\mathcal{H}} = \mathbf{a}_{\text{SC}/E/\mathcal{H}} - \mathbf{a}_{\text{GEO}/E/\mathcal{H}}$ , where

$$\bar{\mathbf{a}}_{\text{GEO}/E/\mathcal{H}} = -\frac{\mu_E}{r_0^3} [r_0, 0, 0]^T \quad (\text{A3})$$

with  $r_0$  as the constant distance between the GEO reference orbit and Earth's center. On the other hand,

$$\mathbf{a}_{\text{SC}/E/\mathcal{H}} = \mathbf{a}_{\text{SC}/E/\mathcal{I}} + 2\boldsymbol{\omega}_{\mathcal{I}/\mathcal{H}} \times \mathbf{v}_{\text{SC}/E/\mathcal{I}} + \boldsymbol{\omega}_{\mathcal{I}/\mathcal{H}} \times (\boldsymbol{\omega}_{\mathcal{I}/\mathcal{H}} \times \mathbf{r}_{\text{SC}/E})$$

where  $\boldsymbol{\omega}_{\mathcal{I}/\mathcal{H}}$  denotes the angular velocity vector of frame  $\mathcal{I}$  relative to frame  $\mathcal{H}$ . Given the constant angular rate of the GEO reference orbit,

$$n_0 = \sqrt{\mu_E/r_0^3} \quad (\text{A4})$$

Note that  $\boldsymbol{\omega}_{\mathcal{I}/\mathcal{H}}$  is resolved in Hill's frame as  $\bar{\boldsymbol{\omega}}_{\mathcal{I}/\mathcal{H}} = [0, 0, -n_0]^T$ , where the constant angular rate of the GEO reference orbit is  $n_0 = \sqrt{\mu_E/r_0^3}$ . Furthermore,  $\bar{\mathbf{r}}_{\text{SC}/\text{GEO}} = [r_1, r_2, r_3]^T$ ,  $\bar{\mathbf{v}}_{\text{SC}/\text{GEO}/\mathcal{H}} = [v_1, v_2, v_3]^T$ , and  $\bar{\mathbf{v}}_{\text{GEO}/E/\mathcal{I}} = [0, v_0, 0]^T$ , where  $v_0 = \sqrt{\mu_E/r_0}$ . Using Eq. (A2),  $\mathbf{a}_{\text{SC}/E/\mathcal{H}}$  is resolved in Hill's frame as follows:

$$\begin{aligned} \bar{\mathbf{a}}_{\text{SC}/E/\mathcal{H}} &= -\frac{\mu_E}{\sqrt{(r_1+r_0)^2+r_2^2+r_3^2}} \begin{bmatrix} r_1+r_0 \\ r_2 \\ r_3 \end{bmatrix} + \begin{bmatrix} 0 \\ 0 \\ -2n_0 \end{bmatrix} \\ &\times \begin{bmatrix} v_1 - n_0 r_2 \\ v_2 + v_0 + n_0 r_1 \\ v_3 \end{bmatrix} + \begin{bmatrix} 0 \\ 0 \\ -n_0 \end{bmatrix} \times \begin{bmatrix} n_0 r_2 \\ -n_0(r_1+r_0) \\ 0 \end{bmatrix} \\ &+ \frac{1}{m_{\text{SC}}} \begin{bmatrix} F_1 \\ F_2 \\ F_3 \end{bmatrix} + \begin{bmatrix} d_{p,1} \\ d_{p,2} \\ d_{p,3} \end{bmatrix} \end{aligned} \quad (\text{A5})$$

where  $\bar{\mathbf{F}} = \mathbf{F}|_{\mathcal{H}} = [F_1, F_2, F_3]^T$  and  $\bar{\mathbf{d}}_p = \mathbf{d}_p|_{\mathcal{H}} = [d_{p,1}, d_{p,2}, d_{p,3}]^T$ . Combining Eqs. (A3–A5) yields

$$\begin{aligned} \bar{\mathbf{a}}_{\text{SC}/\text{GEO}/\mathcal{H}} &= -\frac{\mu_E}{\sqrt{(r_1+r_0)^2+r_2^2+r_3^2}} \begin{bmatrix} r_1+r_0 \\ r_2 \\ r_3 \end{bmatrix} \\ &+ \begin{bmatrix} 2n_0 v_2 + n_0^2 r_1 + \frac{\mu_E}{r_0} \\ -2n_0 v_1 + n_0^2 r_2 \\ 0 \end{bmatrix} + \frac{1}{m_{\text{SC}}} \begin{bmatrix} F_1 \\ F_2 \\ F_3 \end{bmatrix} + \begin{bmatrix} d_{p,1} \\ d_{p,2} \\ d_{p,3} \end{bmatrix} \end{aligned} \quad (\text{A6})$$

For the disturbance term  $\mathbf{d}_p$ , we take into account perturbing accelerations due to the gravity of the moon and sun, the SRP, and  $J_2$  in this paper. Thus,

$$\mathbf{d}_p = \mathbf{d}_{p,M} + \mathbf{d}_{p,S} + \mathbf{d}_{p,\text{srp}} + \mathbf{d}_{p,J_2} \quad (\text{A7})$$

The perturbations due to the gravity of the moon and sun may be obtained according to the three-body problem (spacecraft, Earth, and moon or spacecraft, Earth, and sun, respectively), yielding

$$\mathbf{d}_{p,M} = \mu_M \left( \frac{\mathbf{r}_{M/\text{SC}}}{\|\mathbf{r}_{M/\text{SC}}\|_2^3} - \frac{\mathbf{r}_{M/E}}{\|\mathbf{r}_{M/E}\|_2^3} \right) \quad (\text{A8})$$

$$\mathbf{d}_{p,S} = \mu_S \left( \frac{\mathbf{r}_{S/\text{SC}}}{\|\mathbf{r}_{S/\text{SC}}\|_2^3} - \frac{\mathbf{r}_{S/E}}{\|\mathbf{r}_{S/E}\|_2^3} \right) \quad (\text{A9})$$

where  $\mathbf{r}_{M/\text{SC}}$  and  $\mathbf{r}_{S/\text{SC}}$  are the position vectors of the moon and sun relative to the spacecraft, respectively; and the position vectors of the moon and sun relative to Earth are  $\mathbf{r}_{M/E}$  and  $\mathbf{r}_{S/E}$ , respectively. The gravitational parameters of the moon and sun are denoted by  $\mu_M$  and  $\mu_S$ , respectively. The SRP and  $J_2$  perturbations are given by [19,37]

$$\mathbf{d}_{p,\text{srp}} = -C_{\text{srp}} \frac{S_{\text{SC}}(1 + c_{\text{ref}})}{2m_{\text{SC}}} \frac{\mathbf{r}_{S/\text{SC}}}{\|\mathbf{r}_{S/\text{SC}}\|_2} \quad (\text{A10})$$

$$\mathbf{d}_{p,J2} = \frac{3\mu_E J_2 r_E^2}{2\|\mathbf{r}_{SC/E}\|_2^5} \left[ \left( 5 \frac{\mathbf{r}_{SC/E} \cdot \hat{\mathbf{k}}_{\mathcal{I}}}{\|\mathbf{r}_{SC/E}\|_2^2} - 1 \right) \mathbf{r}_{SC/E} - 2(\mathbf{r}_{SC/E} \cdot \hat{\mathbf{k}}_{\mathcal{I}}) \hat{\mathbf{k}}_{\mathcal{I}} \right] \quad (\text{A11})$$

where  $C_{\text{srp}}$  and  $c_{\text{ref}}$  are constants,  $S_{\text{SC}}$  is the spacecraft's solar-facing area,  $r_E$  is Earth's equatorial radius,  $\hat{\mathbf{k}}_{\mathcal{I}}$  is the three-axis unit vector of frame  $\mathcal{I}$ , and  $J_2 = 1.08264 \times 10^{-3}$ . Now, the discrete-time model is obtained from the continuous-time model given by Eqs. (A6–A11) using Euler's forward method, yielding Eqs. (19) and (20).

## Appendix B: Nonlinear Model for Spacecraft Attitude Control Problem

The nonlinear spacecraft model for the attitude control problem in Sec. IV.B is adopted from [26]. As in Appendix A, for the derivation of the model, a physical vector is denoted by  $\mathbf{r}$  and a physical unit vector is denoted by  $\hat{\mathbf{r}}$ . The mathematical vector  $\mathbf{r}|_{\mathcal{F}}$  is obtained by resolving  $\mathbf{r}$  in a given frame  $\mathcal{F}$ . Two frames are considered: an inertial reference frame denoted by  $\mathcal{I}$ ; and the spacecraft body-fixed frame  $\mathcal{B}$ , which is assumed to be a principal frame. In this section, we use  $\bar{\mathbf{r}} = \mathbf{r}|_{\mathcal{B}}$  to denote  $\mathbf{r}$  resolved in frame  $\mathcal{B}$ . Moreover, the skew-symmetric matrix associated with  $\bar{\mathbf{r}} = [r_1, r_2, r_3]^T$  is defined as

$$S[\bar{\mathbf{r}}] = \begin{bmatrix} 0 & -r_3 & r_2 \\ r_3 & 0 & -r_1 \\ -r_2 & r_1 & 0 \end{bmatrix} \quad (\text{B1})$$

The orientation of frame  $\mathcal{B}$  relative to frame  $\mathcal{I}$  is described by the 3-2-1 Euler angles  $\psi$  (yaw),  $\theta$  (pitch), and  $\phi$  (roll). The continuous-time kinematic equations are given by [38]

$$\begin{bmatrix} \dot{\phi} \\ \dot{\theta} \\ \dot{\psi} \end{bmatrix} = \frac{1}{\cos(\theta)} \begin{bmatrix} \cos(\theta) & \sin(\phi) \sin(\theta) & \cos(\phi) \sin(\theta) \\ 0 & \cos(\phi) \cos(\theta) & -\sin(\phi) \cos(\theta) \\ 0 & \sin(\phi) & \cos(\phi) \end{bmatrix} \bar{\boldsymbol{\omega}}_{\mathcal{B}/\mathcal{I}} \quad (\text{B2})$$

where  $\boldsymbol{\omega}_{\mathcal{B}/\mathcal{I}}$  is the angular velocity of frame  $\mathcal{B}$  relative to  $\mathcal{I}$ , and  $\bar{\boldsymbol{\omega}}_{\mathcal{B}/\mathcal{I}} = [\omega_1, \omega_2, \omega_3]^T$ .

The spacecraft is equipped with  $p$  RWs, where  $\bar{\mathbf{g}}_i$  denotes the unit vector of the  $i$ th RW spin axis resolved in the  $\mathcal{B}$  frame. The spin rate of the  $i$ th RW is  $\nu_i$ , and  $\bar{\boldsymbol{\nu}} = [\nu_1, \nu_2, \dots, \nu_p]^T$ . Moreover, let

$$\mathbf{W} = [\bar{\mathbf{g}}_1, \bar{\mathbf{g}}_2, \dots, \bar{\mathbf{g}}_p] \quad (\text{B3})$$

We assume that all RWs are identical and thin (moments of inertia about axes transversal to the spin axis are approximately zero). The moment of inertia about the RW spin axis is denoted by  $J_w$ , and the moment of the inertia matrix of the spacecraft bus resolved in the  $\mathcal{B}$  frame is given by  $\mathbf{J} = \text{diag}(J_1, J_2, J_3)$ . The locked inertia is defined as

$$\bar{\mathbf{J}} = \mathbf{J} + J_w \mathbf{W} \mathbf{W}^T \quad (\text{B4})$$

The continuous-time rotational dynamics of the spacecraft described in the  $\mathcal{B}$  frame are given by [26]

$$\bar{\mathbf{J}} \dot{\bar{\boldsymbol{\omega}}}_{\mathcal{B}/\mathcal{I}} + S[\bar{\boldsymbol{\omega}}_{\mathcal{B}/\mathcal{I}}] (\bar{\mathbf{J}} \bar{\boldsymbol{\omega}}_{\mathcal{B}/\mathcal{I}} + J_w \mathbf{W} \bar{\boldsymbol{\nu}}) + J_w \mathbf{W} \dot{\bar{\boldsymbol{\nu}}} = \bar{\boldsymbol{\tau}}_{\text{srp}} \quad (\text{B5})$$

where  $\dot{\bar{\boldsymbol{\omega}}}_{\mathcal{B}/\mathcal{I}} = \frac{\mathcal{B}}{\mathcal{B}} \dot{\bar{\boldsymbol{\omega}}}_{\mathcal{B}/\mathcal{I}}$  and  $\dot{\bar{\boldsymbol{\nu}}} = \frac{\mathcal{B}}{\mathcal{B}} \dot{\bar{\boldsymbol{\nu}}}$  are the time derivatives with respect to frame  $\mathcal{B}$  (and resolved in frame  $\mathcal{B}$ ) of the spacecraft and the RW angular velocity vectors, respectively. Note that  $\frac{\mathcal{B}}{\mathcal{B}} \bar{\boldsymbol{\omega}}_{\mathcal{B}/\mathcal{I}} = \frac{\mathcal{I}}{\mathcal{B}} \bar{\boldsymbol{\omega}}_{\mathcal{B}/\mathcal{I}}$  and  $\frac{\mathcal{B}}{\mathcal{B}} \bar{\boldsymbol{\nu}} \approx \frac{\mathcal{I}}{\mathcal{I}} \bar{\boldsymbol{\nu}}$  because the RWs are assumed to rotate orders of magnitude faster than the spacecraft bus, i.e.,  $\|\bar{\boldsymbol{\nu}}\|_1 \gg \|\bar{\boldsymbol{\omega}}_{\mathcal{B}/\mathcal{I}}\|_1$ .

The symbol  $\bar{\boldsymbol{\tau}}_{\text{srp}}$  in Eq. (B5) denotes an external torque due to SRP, which is modeled based on the assumption of a cuboid spacecraft with six flat panels. With  $C_{\text{diff}}$  as the diffusion coefficient, which is assumed to be the same for all panels,  $\beta = (4/9)C_{\text{diff}}$  and  $\kappa = \Phi_S (r_{\text{SC}/S}/r_{E/S})^{-2}/c$  [39], where  $c$  is the speed of light,  $\Phi_S$  is the solar flux acting on the spacecraft,  $r_{E/S} = 1\text{AU}$  is the nominal distance between the Earth and the sun, and  $r_{\text{SC}/S}$  is the distance between the spacecraft and the sun, assuming  $r_{\text{SC}/S} = 0.99\text{AU}$  in this example. Under the assumption that the SRP acts identically across all points on the  $j$ th panel, the SRP acting on panel  $j$  may be expressed as follows [26,39]:

$$\mathbf{P}_j = -\kappa (\hat{\mathbf{q}}_j \cdot \hat{\mathbf{q}}_S) (\hat{\mathbf{q}}_j + \beta \hat{\mathbf{q}}_S) \quad (\text{B6})$$

where  $\hat{\mathbf{q}}_j$  is the normal to the surface of the  $j$ th panel (pointing outward from the spacecraft), and  $\hat{\mathbf{q}}_S$  points from the spacecraft toward the sun. It follows that the SRP torque due to the  $j$ th panel resolved in frame  $\mathcal{B}$  is given by  $\bar{\boldsymbol{\tau}}_{\text{srp},j} = S[\bar{\mathbf{r}}_{j/O} - \bar{\mathbf{r}}_{C/O}] A_j \bar{\mathbf{P}}_j$ , where  $\bar{\mathbf{r}}_{C/O} = [l_x, l_y, l_z]^T$  denotes the position vector of the spacecraft's center of mass  $C$  relative to the geometric center  $O$  of the cuboid. The position vector of the geometric center of the  $j$ th panel relative to  $O$  is given by  $\bar{\mathbf{r}}_{j/O}$ , where  $j \in \{x+, x-, y+, y-, z+, z-\}$ . Thus, we have  $\bar{\mathbf{r}}_{x+/O} = -\bar{\mathbf{r}}_{x-/O} = [L_x/2, 0, 0]^T$ ,  $\bar{\mathbf{r}}_{y+/O} = -\bar{\mathbf{r}}_{y-/O} = [0, L_y/2, 0]^T$ , and  $\bar{\mathbf{r}}_{z+/O} = -\bar{\mathbf{r}}_{z-/O} = [0, 0, L_z/2]^T$ , where the surface areas of the panels are given by  $A_{x+} = A_{x-} = L_y L_z$ ,  $A_{y+} = A_{y-} = L_x L_z$ , and  $A_{z+} = A_{z-} = L_x L_y$ . The total SRP torque is the sum of all panel contributions:

$$\bar{\boldsymbol{\tau}}_{\text{srp}} = \sum_{j=1}^6 \bar{\boldsymbol{\tau}}_{\text{srp},j} I_j \quad (\text{B7})$$

where  $I_j = 1$  if  $\hat{\mathbf{q}}_j \cdot \hat{\mathbf{q}}_S > 0$ , i.e., the  $j$ th panel is facing the sun, and  $I_j = 0$  otherwise.

The nonlinear discrete-time model in Eq. (31) is obtained from the continuous-time model given by Eqs. (B2–B7) using Euler's forward method.

## Acknowledgment

This research is supported by National Science Foundation Award number EECs 1404814.

## References

- [1] Lions, P. L., "Optimal Control of Diffusion Processes and Hamilton–Jacobi–Bellman Equations Part I: The Dynamic Programming Principle and Application," *Communications in Partial Differential Equations*, Vol. 8, No. 10, 1983, pp. 1101–1174. doi:10.1080/03605308308820297
- [2] Barles, G., and Perthame, B., "Exit Time Problems in Optimal Control and Vanishing Viscosity Method," *SIAM Journal on Control and Optimization*, Vol. 26, No. 5, 1988, pp. 1133–1148. doi:10.1137/0326063
- [3] Blanc, A. P., "Deterministic Exit Time Control Problems with Discontinuous Exit Costs," *SIAM Journal on Control and Optimization*, Vol. 35, No. 2, 1997, pp. 399–434. doi:10.1137/S0363012994267340
- [4] Cannarsa, P., Pignotti, C., and Sinestrari, C., "Semiconcavity for Optimal Control Problems with Exit Time," *Discrete and Continuous Dynamical Systems*, Vol. 6, No. 4, 2000, pp. 975–997. doi:10.3934/dcdsa
- [5] Malisoff, M., "Viscosity Solutions of the Bellman Equation for Exit Time Optimal Control Problems with Vanishing Lagrangians," *SIAM Journal on Control and Optimization*, Vol. 40, No. 5, 2002, pp. 1358–1383. doi:10.1137/S0363012900368594
- [6] Kolmanovsky, I. V., and Maizenberg, T. L., "Optimal Containment Control for a Class of Stochastic Systems Perturbed by Poisson and Wiener Processes," *IEEE Transactions on Automatic Control*, Vol. 47, No. 12, 2002, pp. 2041–2046. doi:10.1109/TAC.2002.805679
- [7] Bayraktar, E., Song, Q., and Yang, J., "On the Continuity of Stochastic Exit Time Control Problems," *Stochastic Analysis and Applications*, Vol. 29, No. 1, 2010, pp. 48–60. doi:10.1080/07362994.2011.532020

- [8] Gorodetsky, A. A., Karaman, S., and Marzouk, Y. M., "Efficient High-Dimensional Stochastic Optimal Motion Control Using Tensor-Train Decomposition," *Proceedings of Robotics: Science and Systems*, Rome, Italy, July 2015.  
doi:10.15607/RSS.2015.XI.015
- [9] Buckdahn, R., and Nie, T., "Generalized Hamilton–Jacobi–Bellman Equations with Dirichlet Boundary Condition and Stochastic Exit Time Optimal Control Problem," *SIAM Journal on Control and Optimization*, Vol. 54, No. 2, 2016, pp. 602–631.  
doi:10.1137/140998160
- [10] Zidek, R. A. E., and Kolmanovsky, I. V., "Drift Counteraction Optimal Control for Deterministic Systems and Enhancing Convergence of Value Iteration," *Automatica*, Vol. 83, Sept. 2017, pp. 108–115.  
doi:10.1016/j.automatica.2017.06.015
- [11] Zidek, R. A. E., Bemporad, A., and Kolmanovsky, I. V., "Optimal and Receding Horizon Drift Counteraction Control: Linear Programming Approaches," *American Control Conference (ACC)*, IEEE Publ., New York, 2017, pp. 2636–2641.  
doi:10.23919/ACC.2017.7963350
- [12] Zidek, R. A. E., Petersen, C. D., Bemporad, A., and Kolmanovsky, I. V., "Receding Horizon Drift Counteraction and Its Application to Spacecraft Attitude Control," *27th AAS/AIAA Space Flight Mechanics Meeting*, AAS Paper 17-465, 2017.
- [13] Soop, E. M., *Handbook of Geostationary Orbits*, Vol. 3, Springer Science and Business Media, New York, 1994, Chap. 3.
- [14] Martinez-Sanchez, M., and Pollard, J. E., "Spacecraft Electric Propulsion—An Overview," *Journal of Propulsion and Power*, Vol. 14, No. 5, 1998, pp. 688–699.  
doi:10.2514/2.5331
- [15] Romero, P., and Gambi, J. M., "Optimal Control in the East/West Station-Keeping Manoeuvres for Geostationary Satellites," *Aerospace Science and Technology*, Vol. 8, No. 8, 2004, pp. 729–734.  
doi:10.1016/j.ast.2004.08.004
- [16] Romero, P., Gambi, J. M., and Patiño, E., "Stationkeeping Manoeuvres for Geostationary Satellites Using Feedback Control Techniques," *Aerospace Science and Technology*, Vol. 11, No. 2, 2007, pp. 229–237.  
doi:10.1016/j.ast.2006.08.003
- [17] Lee, B.-S., Hwang, Y., Kim, H.-Y., and Park, S., "East-West Station-Keeping Maneuver Strategy for COMS Satellite Using Iterative Process," *Advances in Space Research*, Vol. 47, No. 1, 2011, pp. 149–159.  
doi:10.1016/j.asr.2010.09.002
- [18] de Bruijn, F. J., Theil, S., Choukroun, D., and Gill, E., "Geostationary Satellite Station-Keeping Using Convex Optimization," *Journal of Guidance, Control, and Dynamics*, Vol. 39, No. 3, 2015, pp. 605–616.  
doi:10.2514/1.G001302
- [19] Weiss, A., Kalabić, U., and Di Cairano, S., "Model Predictive Control for Simultaneous Station Keeping and Momentum Management of Low-Thrust Satellites," *2015 American Control Conference (ACC)*, Inst. of Electrical and Electronics Engineers, New York, 2015, pp. 2305–2310.  
doi:10.1109/ACC.2015.7171076
- [20] Zlotnik, D., Di Cairano, S., and Weiss, A., "MPC for Coupled Station Keeping, Attitude Control, and Momentum Management of GEO Satellites Using On-Off Electric Propulsion," *2017 IEEE Conference on Control Technology and Applications (CCTA)*, IEEE Publ., Piscataway, NJ, 2017, pp. 1835–1840.  
doi:10.1109/CCTA.2017.8062723
- [21] Larson, K. A., McCalmont, K. M., Peterson, C. A., and Ross, S. E., "Kepler Mission Operations Response to Wheel Anomalies," *SpaceOps 2014 Conference*, AIAA Paper 2014-1882, 2014.  
doi:10.2514/6.2014-1882
- [22] Van Cleve, J. E., Howell, S. B., Smith, J. C., Clarke, B. D., Thompson, S. E., Bryson, S. T., Lund, M. N., Handberg, R., and Chaplin, W. J., "That's How We Roll: The NASA K2 Mission Science Products and Their Performance Metrics," *Publications of the Astronomical Society of the Pacific*, Vol. 128, No. 965, 2016, Paper 075002.  
doi:10.1088/1538-3873/128/965/075002
- [23] Crouch, P., "Spacecraft Attitude Control and Stabilization: Applications of Geometric Control Theory to Rigid Body Models," *IEEE Transactions on Automatic Control*, Vol. 29, No. 4, 1984, pp. 321–331.  
doi:10.1109/TAC.1984.1103519
- [24] Tsiotras, P., and Luo, J., "Control of Underactuated Spacecraft with Bounded Inputs," *Automatica*, Vol. 36, No. 8, 2000, pp. 1153–1169.  
doi:10.1016/S0005-1098(00)00025-X
- [25] Tsiotras, P., Shen, H., and Hall, C., "Satellite Attitude Control and Power Tracking with Energy/Momentum Wheels," *Journal of Guidance, Control, and Dynamics*, Vol. 24, No. 1, 2001, pp. 23–34.  
doi:10.2514/2.4705
- [26] Petersen, C. D., Leve, F., Flynn, M., and Kolmanovsky, I., "Recovering Linear Controllability of an Underactuated Spacecraft by Exploiting Solar Radiation Pressure," *Journal of Guidance, Control, and Dynamics*, Vol. 39, No. 4, 2015, pp. 826–837.  
doi:10.2514/1.G001446
- [27] Zavoli, A., De Matteis, G., Giulietti, F., and Avanzini, G., "Single-Axis Pointing of an Underactuated Spacecraft Equipped with Two Reaction Wheels," *Journal of Guidance, Control, and Dynamics*, Vol. 40, No. 6, 2017, pp. 1465–1471.  
doi:10.2514/1.G002182
- [28] Zidek, R. A. E., "Drift Counteraction Optimal Control: Theory and Applications to Autonomous Cars and Spacecraft," Ph.D. Thesis, Univ. of Michigan, Ann Arbor, MI, 2017, Chap. 3.
- [29] Bemporad, A., and Morari, M., "Control of Systems Integrating Logic, Dynamics, and Constraints," *Automatica*, Vol. 35, No. 3, 1999, pp. 407–427.  
doi:10.1016/S0005-1098(98)00178-2
- [30] Richards, A., and How, J., "Mixed-Integer Programming for Control," *2005 American Control Conference (ACC)*, Inst. of Electrical and Electronics Engineers, New York, 2005, pp. 2676–2683.
- [31] Bemporad, A., "Hybrid Toolbox—User's Guide," 2004, <http://cse.lab.imtlucca.it/~bemporad/hybrid/toolbox> [retrieved 17 July 2016].
- [32] "HORIZONS Web-Interface [online database]," Jet Propulsion Lab., Pasadena, CA, 2016, <https://ssd.jpl.nasa.gov/horizons.cgi> [retrieved 14 Nov. 2015].
- [33] Goebel, D., Martinez-Lavin, M., Bond, T., and King, A., "Performance of XIPS Electric Propulsion in On-Orbit Station Keeping of the Boeing 702 Spacecraft," *38th AIAA/ASME/SAE/ASEE Joint Propulsion Conference and Exhibit*, AIAA Paper 2002-4348, 2002.  
doi:10.2514/6.2002-4348
- [34] Wie, B., *Space Vehicle Dynamics and Control*, AIAA, Reston, VA, 2008, pp. 100, 223, 299–300.
- [35] Zidek, R. A. E., and Kolmanovsky, I. V., "Approximate Closed-Form Solution to a Linear Quadratic Optimal Control Problem with Disturbance," *Journal of Guidance, Control, and Dynamics*, Vol. 40, No. 2, 2017, pp. 477–483.  
doi:10.2514/1.G001666
- [36] Earl, M. G., and D'andrea, R., "Iterative MILP Methods for Vehicle-Control Problems," *IEEE Transactions on Robotics*, Vol. 21, No. 6, 2005, pp. 1158–1167.  
doi:10.1109/TRO.2005.853499
- [37] Bate, R. B., Mueller, D. D., and White, J. E., *Fundamentals of Astrodynamics*, Dover, New York, 1971, Chap. 9.7.
- [38] Hughes, P. C., *Spacecraft Attitude Dynamics*, Courier Corp., North Chelmsford, MA, 2004, Chap. 2.
- [39] Linares, R., Jah, M. K., Crassidis, J. L., Leve, F. A., and Kececy, T., "Astrometric and Photometric Data Fusion for Inactive Space Object Mass and Area Estimation," *Acta Astronautica*, Vol. 99, June–July 2014, pp. 1–15.  
doi:10.1016/j.actaastro.2013.10.018